Brainstem nucleus incertus controls contextual memory formation

András Szőnyi[1,2], Katalin E. Sos[1,2], Rita Nyilas[3], Dániel Schlingloff[1,2], Andor Domonkos[1], Virág T. Takács[1], Balázs Pósfai[1,2], Panna Hegedüs[1,2], James B. Priestley[3], Andrew L. Gundlach[4], Attila I. Gulyás[1], Viktor Varga[1], Attila Losonczy[3], Tamás F. Freund[1] and Gábor Nyiri[1]*

1: Laboratory of Cerebral Cortex Research, Department of Cellular and Network Neurobiology, Institute of Experimental Medicine, Hungarian Academy of Sciences, Budapest, Hungary

2: János Szentágothai Doctoral School of Neurosciences, Semmelweis University, Budapest, Hungary

3: Department of Neuroscience, Mortimer B. Zuckerman Mind Brain Behavior Institute, Kavli Institute for Brain Science, Columbia University, New York, NY, USA

4: Peptide Neurobiology Laboratory, The Florey Institute of Neuroscience and Mental Health, Parkville, Victoria, Australia

*Corresponding author, e-mail: nyiri.gabor@koki.mta.hu

Abstract

Hippocampal pyramidal cells encode memory engrams which guide adaptive behavior. Selection of engram-forming cells is regulated by somatostatin-positive dendrite-targeting interneurons, which inhibit pyramidal cells that are not required for memory-formation. Here, we found that GABAergic neurons of the mouse *nucleus incertus* (NI) selectively inhibit somatostatin-positive interneurons in the hippocampus, both mono-synaptically and indirectly via the inhibition of their sub-cortical excitatory inputs. We demonstrated that NI GABAergic neurons receive monosynaptic inputs from brain areas processing important environmental information, and their hippocampal projections are strongly activated by salient environmental inputs in vivo. Optogenetic manipulations of NI GABAergic neurons can shift hippocampal network state and bidirectionally modify the strength of contextual fear memory formation. Our results indicate that brainstem NI GABAergic cells are essential for controlling contextual memories.

Introduction

Fear memories, which allow mice to avoid future aversive events, are formed by associating aversive stimuli (unconditioned stimulus, US) with their environmental context. The dorsal hippocampus (HIPP) plays an essential role in contextual memory encoding and transmits this information mainly via CA1 pyramidal neurons to the cortex (*1*–*3*). Dorsal CA1 pyramidal neurons receive the unified representation of the multisensory context at their proximal dendrites from the CA3 subfield inputs (*4*), while the discrete sensory attribute of the aversive stimulus (US) is primarily conveyed by the direct temporo-ammonic pathway to their distal dendrites (*5*–*7*). At the cellular level, the dendritic interactions of these inputs may result in long-term synaptic plasticity in CA1 pyramidal neurons (*8*–*10*), a subset of which can form memory engrams to encode contextual fear memories (*11*). Both intact contextual information processing and direct sensory information related inputs are required for precise episodic memory formation (*12*–*14*).

The number of dorsal CA1 pyramidal neurons participating in the formation of a given memory engram component must be delicately balanced (*15*). The majority of pyramidal cells must be inhibited, (i.e., excluded from memory encoding at the moment of memory formation), because if the US information reaches too many pyramidal cells, engrams may lack specificity, which may engender memory interference (*16*, *17*). Exclusion of US information in hippocampal CA1 is achieved by somatostatin (SOM) expressing *oriens-lacunosum moleculare* (OLM) inhibitory interneurons (*16*). OLM cells establish far the most abundant local SOM-positive synapses (*16*, *18*). OLM cells selectively inhibit the distal dendrites of CA1 pyramidal neurons, which receive the primary sensory-related inputs from the entorhinal cortex, representing the US (*19*–*22*). Indeed, artificial silencing of dorsal CA1 SOM-positive neurons at the moment of US presentation disrupts fear learning (*16*, *17*). OLM cell activity is synchronized with the US via cholinergic and glutamatergic excitatory inputs from the medial septum (MS) and diagonal bands of Broca. Cholinergic neurons are rapidly and reliably recruited by salient environmental stimuli (*16*, *23*) and strongly innervate hippocampal OLM neurons (*3*, *16*, *21*), while MS glutamatergic neurons display locomotion-related activity increases, and also innervate hippocampal OLM cells (*22*, *24*).

Conversely, if too many pyramidal neurons are inhibited, allocation to engrams may be insufficient and memory formation would be impaired (*25*). Thus, to balance the sparsity of hippocampal engrams, activation of OLM neurons must be adequately controlled. Inhibitory regulation of OLM neurons would ideally arise also from an extra-hippocampal area that integrates relevant environmental information, yet the source of such balancing inhibitory input to OLM neurons was, until now, unknown.

The pontine *nucleus incertus* (NI), characterized by expression of the neuropeptide, relaxin-3 (*26*–*28*), sends an ascending GABAergic pathway to the septo-hippocampal system. NI neurons display activity related to hippocampal theta rhythm and are thought to play an important role in stress and arousal (*29*–*34*).

Here, using cell type-specific neuronal tract-tracing, immunogold receptor localization and electrophysiological methods, we discovered that NI GABAergic neurons selectively inhibit hippocampal SOM-

positive neurons both mono-synaptically and also indirectly via inhibition of excitatory glutamatergic and cholinergic neurons in the MS. Using monosynaptic rabies-tracing, we observed that NI receives direct inputs from several brain areas that process salient environmental stimuli, and indeed, using in vivo two-photon calcium imaging in head-fixed awake mice, we demonstrated that such stimuli rapidly activated hippocampal fibers of NI GABAergic neurons. Behavioral conditioned fear experiments revealed that optogenetic stimulation of NI GABAergic cells or their fibers in the dorsal HIPP, precisely at the moment of US presentation, prevented the formation of contextual fear memories. In parallel, optogenetic stimulation of NI GABAergic neurons decreased the power and frequency of the encoding-related hippocampal theta rhythm in vivo. In contrast, optogenetic inhibition of NI GABAergic neurons during fear conditioning, resulted in the formation of excessively enhanced contextual memories. These findings demonstrate the fundamental importance of NI GABAergic neurons in hippocampus-dependent episodic memory formation.

Results

NI GABAergic neurons selectively inhibit hippocampal SOM-positive interneurons

We injected Cre-dependent adeno-associated tracer virus (AAV5, see Supplementary Materials and Methods) into the NI of vesicular GABA transporter (vGAT)-Cre mice to reveal the projections of GABAergic neurons of NI (Fig. 1A). It demonstrated that NI GABAergic fibers selectively project to the *stratum oriens* of the HIPP and the *hilus* of the dentate gyrus (Fig. 1B). SOM neurons are typically found only in these sub-regions of HIPP (*35*). GABAergic NI nerve terminals were all positive for the neuropeptide, relaxin-3 (Fig. 1C). Double retrograde tracing in wild-type (WT) mice, using the retrograde tracers FluoroGold (FG) and Choleratoxin B (CTB), revealed that NI and HIPP are connected almost exclusively ipsilaterally (Fig. S1A-C). Using Cre-dependent AAV5 viral tracing, we also confirmed that brainstem areas surrounding NI do not send GABAergic projections to the HIPP (Fig. S2A-F) and NI GABAergic neurons do not use glutamate, glycine, acetylcholine, serotonin or other monoamines as neurotransmitters (Fig. S2G-J).

To identify the targets of NI GABAergic fibers in the HIPP, we injected Cre-dependent AAV5 tracer virus into the NI of vGAT-Cre-tdTomato reporter mice (Supplementary Materials and Methods and Fig. S1D). Double immunoperoxidase reactions and correlated light- and electron microscopy revealed that NI fibers establish synaptic contacts with tdTomato-expressing GABAergic interneurons in the HIPP (at least 87% were identified as interneurons, Fig. S1E). Then, using Cre-dependent AAV5 viral-labeling of SOM interneurons in SOM-Cre mice, we found that most of the relaxin-3 positive NI terminals (at least 62%) targeted SOM-positive cells (Fig. 1D-E). The vast majority of SOM-positive CA1 fibers are present in *stratum lacunosum-moleculare*, which clearly indicated that they originate from OLM cells as described before (*16*, *18*, *36*). Using Cre-dependent AAV5 viral-labeling in vGAT-Cre mice, we observed that NI GABAergic fibers establish symmetrical synapses typically with SOM-positive

interneurons (Fig. 1F-H) that also contain the previously identified markers (*37*) metabotropic glutamate receptor 1α (mGluR1α) and parvalbumin (PV, Fig. S1F-H). These results demonstrate that the primary target of NI fibers in the HIPP are the dendrite-targeting SOM-positive interneurons, the local effect of which neurons mostly originate from OLM cells. Using a combination of CTB and Cre-dependent AAV5 in vGAT-Cre mice, we observed that some SOM positive GABAergic interneurons in the HIPP, which project to the subiculum or the MS (*38*, *39*) also receive contacts from the NI (Supplementary Materials and Methods and Fig. S1I-P).

Using correlated light- and immuno-electron microscopic analysis, we found that the synapses of NI fibers are symmetrical, contain $GABA_A$-receptor γ2 subunits and the GABAergic synapse specific scaffolding protein gephyrin, postsynaptically in the HIPP (Fig. 1I).

To investigate the functional properties of these GABAergic synapses, we injected channelrhodopsin (ChR2) containing Cre-dependent AAV5 into the NI of vGAT-Cre mice and 6-12 weeks later, we cut horizontal slices from the HIPP for in vitro optogenetic experiments (Fig. 1J, Supplementary Materials and Methods, Fig. S3A, Fig. S4A). Light stimulation of hippocampal NI GABAergic fibers reliably evoked gabazine-sensitive inhibitory postsynaptic potentials (IPSCs) from voltage-clamped interneurons located to the *stratum oriens* of CA1 (Fig. 1K-N, Fig. S3B-C), indicating $GABA_A$-receptor-dependent GABAergic neurotransmission in these synapses. Although NI GABAergic neurons express relaxin-3 and HIPP SOM neurons express its receptor (*28*, *40*), gabazine could block all currents at these time scales. Recorded neurons were filled with biocytin and *post-hoc* neurochemical analysis of filled neurons revealed that at least 12 of 18 cells were clearly SOM-positive (Fig. 1K). Although not all recorded neurons could be fully morphologically reconstructed, 6 of them were unequivocally identified as typical dendrite-targeting OLM neurons (Fig. 1M). Altogether we found, that 14 out of 18 randomly recorded and NI GABAergic cells targeted neurons were either SOM-positive or SOM-false-negative OLM cells, suggesting that at least 78% of the target cells are SOM-positive. Whereas, in immunohistochemistry described above, this number was at least 62%. Because only 14% of CA1 interneurons are SOM-positive (*41*), these numbers suggest a very high target specificity for SOM-containing interneurons. Light stimulation suggested that NI GABAergic synapses display short-term synaptic depression at higher stimulation frequencies (30-50 Hz: Fig. S3C) that was not observed at lower frequencies (5-20 Hz: Fig. S3C). These data clearly demonstrate that NI fibers directly target SOM positive dendrite-targeting OLM interneurons in the HIPP with functional GABAergic synapses.

NI GABAergic neurons inhibit MS neurons that excite OLM interneurons

HIPP SOM neurons receive their main extra-hippocampal excitatory inputs from glutamatergic and cholinergic neurons of the MS (*16*, *21*, *22*). We hypothesized that NI may also inhibit HIPP SOM-positive OLM cells indirectly, by inhibition of these excitatory input neurons in the MS.

Using Cre-dependent AAVs to label GABAergic NI neurons in vGAT-Cre mice (Fig. 2A), we determined that MS is strongly innervated by relaxin-3 positive NI GABAergic fibers (Fig. 2B-C). NI neurons established $GABA_A$-

receptor γ2 subunit-positive and gephyrin-positive symmetrical synapses in MS (Fig. 2D). Using Cre-dependent AAV5 viral tracing we also confirmed that brainstem areas surrounding NI do not send GABAergic projections to the MS (Fig. S2A-H).

To investigate, whether GABAergic NI fibers target the glutamatergic or cholinergic cells in the MS, we injected Cre-dependent AAV5 into the NI of vesicular glutamate transporter 2 (vGluT2)-Cre (Fig. 2E) or choline acetyltransferase (ChAT)-Cre (Fig. 2G) mice. These experiments revealed that relaxin-3 positive terminals of the NI frequently establish gephyrin-positive synapses on glutamatergic (at least 55%, Fig. 2F) and cholinergic (at least 8%, Fig. 2H) cells in the MS, indicating that NI projections can also inhibit the main extra-hippocampal excitatory input to hippocampal OLM cells.

In addition, we performed double retrograde tracing by injecting FG into the MS and CTB into the HIPP of WT mice bilaterally (Fig. 2I-J). We observed that many (at least 37%) of the individual NI GABAergic neurons that target HIPP also send axon collaterals to the MS (Fig. 2K). These data indicate that NI GABAergic neurons can synchronously inhibit HIPP OLM cells both directly in HIPP, and also indirectly by inhibition of their excitatory afferents in the MS.

NI GABAergic fibers in HIPP are rapidly activated by salient environmental stimuli in vivo

These anatomical and in vitro physiological data indicated that NI GABAergic neurons would be ideal to counterbalance the MS activation of OLM cells, which would permit fine-tuned regulation of pyramidal cell participation in memory formation. To test, whether NI GABAergic neurons indeed respond to sensory stimuli and behavioral state, we combined two-photon (2P) calcium imaging with behavioral monitoring in awake mice. We injected AAV2/1-EF1a-DIO-GCaMP6f into the NI of vGAT-Cre mice and implanted a chronic imaging window superficial to the dorsal CA1 of the HIPP (Fig. 3A). After recovery, water restriction and habituation to head-restraint, we engaged mice in two different behavioral paradigms, while imaging the fluorescent activity of GCaMP6f-positive NI boutons in the *stratum oriens* of the dorsal CA1 (Fig. 3B-C).

In the first experiment, the random foraging task, mice ran on a cue-less burlap belt in search of water rewards, which were delivered at 3 random locations on each lap. Bouton fluorescence was elevated during periods of running (Fig. 3D), consistent with previous observations of increased neural activity in the NI during hippocampal theta rhythm (*32*). To investigate how calcium dynamics in NI GABAergic axon terminals are modulated by locomotion state transitions, we examined GCaMP6f fluorescence changes in NI-GABAergic boutons in relation to the onset and offset of locomotion. We calculated peri-event time histograms (PETHs) aligned to running-start and running-stop events (Fig. 3E) and found that the majority of dynamic NI boutons were similarly modulated by the onset and offset of running (Fig. 3H).

In the second behavioral paradigm, the salience task, we explored whether discrete stimuli of various sensory modalities also modulate the activity of NI GABAergic axonal boutons in the HIPP, while the mouse was

stationary (*16*, *42*). The movements of mice were restrained while different sensory cues (aversive air-puffs, water rewards, auditory tones and light flashes) were randomly presented to them (Fig. 3B, F). We calculated peri-stimulus time histograms (PSTHs) and observed calcium responses in NI boutons to all types of stimuli. Salient stimuli with special valence such as aversive air-puff and water reward had particularly strong effects on bouton calcium dynamics (Fig. 3F), and also activated a larger fraction of NI boutons (Fig. 3I).

Finally, to determine the stimulus-dependent variability of the responses of NI terminals in the HIPP, we analyzed the Jaccard similarity of boutons in the salience experiments, based on their stimulus preference. Although all stimuli recruited an overlapping population of boutons, we detected some differences between the activated bouton populations (Fig. 3J).

NI GABAergic neurons receive monosynaptic inputs from areas processing salient environmental stimuli

Above mentioned data demonstrate that NI GABAergic neurons transmit information on salient environmental modalities from the brainstem to the HIPP. To directly identify upstream brain areas containing neurons that synaptically target the GABAergic neurons of NI, we used mono-trans-synaptic rabies tracing (*43*). We used Cre-dependent helper viruses and G-protein deleted rabies virus in vGAT-Cre mice (Supplementary Materials and Methods, Fig. 4A). These studies assessed the level of convergence onto NI GABAergic neurons, and thus the type of inputs that can fine-tune HIPP memory formation via the modulation of NI GABAergic cells. The specificity of the virus expression was tested in WT mice (Fig. 4B).

We detected an extensive convergence of inputs onto NI GABAergic neurons, with prominent synaptic inputs from several brain areas highly relevant to associated behaviors, including the prefrontal cortex, lateral habenula, zona incerta, mammillary areas, and raphe regions. These afferent regions play essential roles in movement, aversive or rewarding stimulus processing, and memory encoding (Fig. 4C, for details see Table S6). We did not find rabies labeled neurons in the HIPP, confirming the lack of direct output from HIPP to NI.

Rabies labeling revealed that NI GABAergic neurons are targeted by the lateral habenula (LHb; Fig. 4C), which plays a fundamental role in aversive behavior (*44*, *45*). To confirm that the glutamatergic neurons of the LHb target the NI, we injected Cre-dependent AAV5 into the LHb of vGluT2-Cre mice (Fig. 4D-E) and detected strong fiber labeling in NI (Fig. 4F).

Rabies tracing also revealed that NI GABAergic neurons receive a strong monosynaptic input from the median raphe region (MRR, Fig. 4C, Table S6). HIPP memory formation is sensitive to stress, and NI neurons express functional corticotrophin-releasing hormone (CRH) receptor 1 that plays a role in stress processing (*32*, *46*). MRR contains a small CRH-positive cell population (*47*). Injection of Cre-dependent AAV5 into the MRR of CRH-Cre mice (Fig. 4G-H) revealed that MRR is a prominent source of CRH signaling in the NI (Fig. 4I).

MS cholinergic neurons are known to transmit a rapid and precisely timed attention signal to cortical areas (*23*), while the activity of MS glutamatergic (vGluT2-positive) neurons is correlated with movement and HIPP theta

rhythm (*22*, *24*). We observed that virtually none of the NI projecting rabies-labeled MS neurons were positive for ChAT, parvalbumin or calbindin (Table S7). Injections of Cre-dependent AAV5 into the MS of ChAT-Cre mice confirmed the lack of cholinergic innervation of NI from MS.

Because vGluT2 is not detectable in neuronal cell bodies, we directly labeled MS vGluT2 positive glutamatergic cells, using injections of Cre-dependent AAV5 into the MS of vGluT2-Cre mice (Fig. 4J-K) and observed that MS glutamatergic neurons provide a strong input into the NI (Fig. 4L).

NI GABAergic cells regulate hippocampal network activity

HIPP theta activity is essential for contextual memory formation (*25*, *48*) and typical during exploration (*49*, *50*), therefore, we investigated the effects of NI GABAergic neurons on HIPP theta activity. We injected ChR2-containing Cre-dependent AAV5 into the NI of vGAT-Cre mice. Later, we implanted an optic fiber over the NI (Fig. S4A) and placed a multichannel linear probe into the dorsal HIPP (Fig. 5A-D). After recovery and habituation, HIPP rhythmic activities were recorded in an open field or on a linear track, where mice could behave freely (Fig. 5B). Blue light stimulation was triggered by the experimenter during every recording condition, while electrophysiological activity in HIPP was continuously recorded.

As revealed by wavelet analysis of the HIPP local field potentials (LFP), stimulation of NI GABAergic neurons significantly decreased the power of HIPP theta activity (Fig. 5E-G, Fig. S5A-D), while no such effect occurred after introduction of light into a dummy fiber implanted in the same mice (Supplementary Materials and Methods, Fig. 5E-G, Fig. S5C-D). The effect was most prominent in the high theta range (8-12Hz), less in the low theta range (5-8Hz), while it was generally stronger when mice actively explored their environment (Fig. 5G). Stimulation of NI GABAergic neurons also reduced HIPP theta power during REM sleep (Fig. S5D-E). Current source density analysis revealed a prominent effect on the magnitude of apical dendritic sinks and sources, excluding the possibility of general silencing of CA1, instead implying a stimulus-triggered alteration of excitation – inhibition balance (Fig. S5F-I). Importantly, none of these effects were observed when we stimulated the NI GABAergic neurons in urethane-anaesthetized mice.

NI GABAergic neurons bi-directionally regulate hippocampus-dependent contextual memory formation

Our findings above indicated that NI GABAergic neurons can integrate behavioral modalities from several key brain areas and are activated by salient environmental inputs, while they inhibit HIPP OLM cells both directly and indirectly. These findings suggest that this brainstem projection is ideally suited to provide the sub-cortical inhibition of these HIPP SOM-positive dendrite-targeting neurons for balancing the selection of HIPP pyramidal cells that participate in memory formation.

To test this possibility, first we injected ChR2-containing Cre-dependent AAV5 (ChR2-mice) or control Cre-dependent AAV5 (CTRL-mice) into the NI of vGAT-Cre mice and implanted an optic fiber over the NI (Fig. 6A, Fig.

S4A). After handling, mice were placed into a new multisensory context (environment “A”), where they received four foot-shocks and light stimulation of NI precisely aligned to foot-shocks (Supplementary Materials and Methods, Fig. 6A). All mice displayed equally strong immediate reactions to foot-shocks. 24 h later, mice were placed into the same environment “A”, where CTRL-mice displayed strong freezing behavior as expected, while ChR2-mice displayed almost no freezing behavior (Fig. 6A). An elevated plus-maze test, 1 hour later, revealed significantly lower anxiety levels in ChR2-mice compared to CTRL-mice (Fig. 6A). These findings indicated that contextual fear memory formation can be severely impaired or blocked if NI GABAergic neurons are strongly activated precisely at the time of US presentation.

In an additional control experiment, we conducted the same contextual fear conditioning experiment with the same cohorts of ChR2- and CTRL-mice one week later, in a different environment “B” (Fig. S6A) without light stimulations. On the second day of the experiment, both ChR2- and CTRL-mice displayed high freezing behavior (Fig. S6A-B), confirming that ChR2-mice could also display appropriate fear behavior.

To confirm that NI GABAergic cells act directly on HIPP SOM-positive cells, we created a second cohort of ChR2- and CTRL-mice as described above (Fig. 6B). However here, optic fibers were implanted bilaterally above the dorsal HIPP (Fig. 6B, Fig. S4A-B). In similar contextual fear conditioning experiments described above, ChR2-mice again displayed significantly lower freezing levels in environment “A”, where they received NI light stimulation during foot-shocks, than in environment “B”, where NI was not stimulated (Fig. 6B). This effect was absent in CTRL mice (Fig. 6B). These results suggest that dorsal HIPP fibers of NI GABAergic neurons can inhibit the formation of contextual memory directly in the HIPP.

The balancing of the selection of pyramidal cells that associate US with environmental context should be timed precisely during US presentation. To test the importance of timing, we injected ChR2-containing Cre-dependent AAV5 into the NI of vGAT-Cre mice and implanted an optic fiber over the NI (Fig. 6C, Fig. S4A). Mice were divided into two groups: one group received NI GABAergic neuron stimulation aligned to foot-shocks as described above (“light-aligned-mice”), while a second group received light stimulation exactly between foot-shocks (i.e. 15 seconds after each foot-shock, “light-shifted-mice”, Fig. 6C). “Light-shifted-mice” displayed significantly higher freezing levels compared to “light-aligned-mice”, indicating that activation of NI GABAergic neurons needs to occur precisely during US presentation to be effective (Fig. 6C).

Finally, we investigated whether inhibition of NI GABAergic neurons during contextual fear conditioning induced opposite effects, i.e. whether it can create inadequately strong fear. We injected archaerhodopsinT-3 (ArchT 3.0)-containing Cre-dependent AAV5 (ArchT-mice) or control Cre-dependent AAV5 (CTRL-mice) into the NI of vGAT-Cre mice and implanted an optic fiber over the NI (Fig. 6D, Fig. S3D and Fig. S4A). After handling, mice were tested in a delay cued fear conditioning paradigm. First, we placed mice into environment “A”, where they received three auditory tones, at the end of which mice received foot-shocks. NI received a constant yellow light during the experiments. 24 h later, mice were placed back into environment “A” to test their hippocampus-

dependent contextual fear memories. We observed that ArchT-mice displayed significantly stronger freezing behavior than CTRL-mice (Fig. 6D). The auditory cue dependent fear component of established fear memories is known to be hippocampus-independent (*51*). Therefore, on the next day, we placed these mice into a different neutral environment "B" and presented them with the auditory cues (Fig. 6D). At this time, however, we found no difference between the freezing levels of the two groups, further suggesting that the effect of NI GABAergic neurons on contextual memory formation was hippocampus-dependent.

Discussion

Encoding of episodic memories is essential for the survival of animals. HIPP pyramidal neurons of the dorsal CA1 region play a key role in this process (*1*, *25*, *52*), by pairing multisensory contextual information with direct sensory-related inputs (e.g. an US) at the cellular level, via long-term synaptic plasticity mechanisms (*8*, *10*, *15*). However, if too many pyramidal neurons receive the same direct sensory-related inputs, information pairing is not specific enough and the memory trace will be lost (*16*). Therefore, only a subpopulation of pyramidal neurons participate in this process by forming cell-assemblies that encode memory engrams (*11*, *15*), while the direct sensory-related input must be excluded from most of the pyramidal neurons (*16*).

HIPP SOM-positive OLM neurons selectively inhibit the distal dendrites of pyramidal neurons to filter out direct sensory-related excitatory inputs from the entorhinal cortex (*3*, *16*, *22*). Upon salient environmental stimuli, OLM cells are activated by glutamatergic and cholinergic inputs from the MS (*3*, *16*, *19*–*22*), therefore dendrite-targeting OLM cells can efficiently block direct sensory-related inputs to most pyramidal cells at the time of memory formation, thereby leaving only a subpopulation of pyramidal neurons to form engrams.

However, the selection of these pyramidal neurons must be precisely balanced. We hypothesized that dorsal CA1 dendrite-targeting OLM interneurons should also be precisely inhibited in time based on sub-cortical information, because otherwise, under-recruitment of pyramidal neurons will lead to unstable engrams (*17*, *25*, *52*). We discovered that NI GABAergic neurons are well suited to counter-balance the activation of OLM cells in a time- and sensory stimulus-dependent manner.

We demonstrated that NI GABAergic neurons receive monosynaptic inputs from several brain areas that process salient environmental stimuli and that they are activated rapidly by such stimuli in vivo. We revealed that these NI GABAergic neurons provide a selective, direct inhibition of HIPP SOM-positive interneurons, the vast majority of which CA1 fibers originate from dendrite-targeting OLM interneurons (*16*, *18*). Although other types of HIPP neurons have little contribution to the local SOM-positive innervation of the CA1 area, some SOM-positive *bistratified* interneurons may also support the inhibition of pyramidal cell dendrites, in addition to extra-hippocampal projecting GABAergic neurons, the rare local collaterals of which also target pyramidal cell dendrites (*53*).

MS cholinergic cells release GABA, immediately followed by a strong cholinergic excitatory component (*54*), which results in an effective net activation of OLM cells (*16*). Here we revealed that medial septal glutamatergic and cholinergic excitatory inputs to OLM neurons are also inhibited by NI GABAergic neurons simultaneously, which facilitates the effective and precisely timed inhibition of hippocampal OLM cells. We also demonstrated that many of these direct and indirect inhibitory actions are provided by collaterals of the same NI GABAergic neurons, further facilitating a highly synchronous inhibition.

Although OLM cells in intermediate and ventral HIPP seem to regulate memory formation differently (*17*), previous studies agree that direct inhibition of dorsal CA1 OLM neurons resulted in weaker memory formation (*16*, *17*). Indeed, we found that dorsal CA1 OLM neurons can be inhibited by activating brainstem NI GABAergic neurons. Our behavioral data revealed that the precisely-timed activation of NI GABAergic neurons could lead to an almost complete inhibition of the formation of contextual fear memories.

In contrast, NI-lesioned rats display pathologically strong memory formation, indicated by impaired fear extinction and increased fear generalization (*55*, *56*). In this regard, we also observed stronger contextual fear memory formation after inhibition of GABAergic NI neurons.

We described that NI GABAergic neurons receive monosynaptic inputs from several brain areas that process salient environmental stimuli and our analysis of our 2P calcium imaging data revealed that different environmental inputs activated different fractions of NI fibers. Emotionally more salient inputs were more effective. Furthermore, our Jaccard similarity analysis suggested that NI fibers may be activated by different sensory stimuli. Previous studies have also shown heterogeneity amongst the NI cells based on their activity patterns or based on their CRH receptor / relaxin-3 content (*30*, *32*). Therefore, one may speculate that different subset of NI GABAergic neurons could enforce the disinhibition of a different subset of pyramidal neurons, leading to the selection of different sets of memory-encoding pyramidal cell populations, which would be beneficial to encode different contextual memories more specifically.

The activity of medial septal glutamatergic neurons is positively correlated with the running speed of the animal and with the frequency of hippocampal theta rhythm (*22*, *24*, *57*). NI neurons also display firing phase-locked to hippocampal theta (*32*, *58*, *59*). Our results reveal that MS glutamatergic neurons innervate the NI, and that the activity of NI GABAergic fibers is elevated during running, active exploration and new episodic memory formation. Therefore, MS glutamatergic neurons may support the phase-locking of NI GABAergic neurons to HIPP theta rhythm.

We observed that activation of NI GABAergic neurons partly inhibited and reorganized HIPP theta rhythmic activity, which rhythm is known to be essential for episodic memory formation (*25*), further suggesting a role of NI GABAergic neurons in memory formation. This effect on theta activity may be facilitated by one of the different populations of septo-hippocampal parvalbumin-positive GABAergic neurons (*60*–*63*). Although it is unclear, which one of them receives GABAergic synapses from NI, some of them express metabotropic relaxin-3 receptors and

may be inhibited by NI (*64*, *65*). Different types of MS parvalbumin cells target different HIPP interneurons in a rhythmic fashion and they mostly target HIPP basket cells that are known to be fundamental in modulating HIPP theta rhythms (*63*, *66–68*).

In the rat, NI GABAergic neurons that express CRH-R1 are activated by different stressors (*29*, *32*, *33*, *56*). Our results demonstrate that NI GABAergic neurons receive inputs from several brain areas, some of them related to stress regulation, and amongst which, the projection from CRH-expressing neurons of the median raphe region, was previously unknown. Therefore, CRH-dependent activation of NI GABAergic neurons might contribute to impaired episodic memory formation observed under stressful conditions (*46*, *69*).

Pathological neurodegeneration of NI GABAergic neurons may result in hyperthymesia-like symptoms, in which the unnecessarily encoded detailed memories of everyday life cause cognitive problems in patients (*70*, *71*). NI GABAergic neuron dysfunction may also contribute to general anxiety-like syndromes or post-traumatic stress disorders, where pathologically strong episodic memory formation is present. On the other hand, over-activity of NI GABAergic neurons may lead to dementia-like disorders.

An important physiological role of NI GABAergic neurons may be the fine-tuning of the selection of memory-encoding pyramidal cells, based on the relevance and/or modality of environmental inputs. NI GABAergic neurons may also help filter out non-relevant everyday experiences, to which animals have already accommodated, by regulating the population sparsity of memory-encoding dorsal CA1 pyramidal neurons. Our data represent an unexpectedly specific role of an ascending inhibitory pathway from a brainstem nucleus in memory encoding.

Methods Summary

Ethical considerations and used mouse strains

All experiments were performed in accordance with the Institutional Ethical Codex and the Hungarian Act of Animal Care and Experimentation guidelines (40/2013, II.14), which are in concert with the European Communities Council Directive of September 22, 2010 (2010/63/EU). All two-photon (2P) imaging experiments were conducted in accordance with the United States of America, National Institutes of Health guidelines and with the approval of the Columbia University Institutional Animal Care and Use Committee. The following mouse strains were used in the experiments: C57Bl/6J wild type, ChAT-iRES-Cre, CRH-iRES-Cre, vGAT-iRES-Cre, vGAT-iRES-Cre::Gt(ROSA26)Sor-CAG/tdTomato, vGluT2-iRES-Cre (*72*), GlyT2-iRES-Cre and SOM-iRES-Cre. We used at least 6 weeks-old mice from both genders in our experiments.

Stereotaxic surgeries for viral gene transfer and retrograde tracing

Mice were deeply anesthetized and were then mounted and microinjected using a stereotaxic frame. We used one of the following viruses: AAV2/1-EF1a-DIO-GCaMP6f; AAV2/5-EF1α-DIO-eYFP; AAV2/5-EF1α-DIO-

mCherry; AAV2/5-CAG-FLEX-ArchT-GFP; AAV2/5-EF1α-DIO-hChR2(H134R)-eYFP. For retrograde tracing experiments we injected 2% FluoroGold or 0.5% Cholera toxin B subunit into the target areas. The coordinates for the injections were defined by a stereotaxic atlas (*73*).

Hippocampal cranial window implants for two-photon imaging experiments

We implanted an imaging window/head-post as described previously (*16*). Briefly, under anesthesia, a 3-mm diameter craniotomy was made in the exposed skull over the left dorsal hippocampus and the underlying cortex was slowly aspirated. A custom-made sterilized cylindrical steel imaging cannula with a glass cover slip window (3-mm diameter × 1.5-mm height, as described in (*42*)) was inserted into the craniotomy and was cemented to the skull. Analgesia was administered during and after the procedure for three days.

Optic fiber implantations for behavioral experiments

For behavioral experiments, optic fibers were implanted into the brain. Their positions are illustrated in Fig. S4A-B. After the surgeries, mice received meloxicam analgesia, and were placed into separate cages until experiments or perfusions.

Stereotaxic surgeries for electrophysiological recordings in freely moving mice

AAV2/5-EF1a-DIO-hChR2(H134R)-YFP transfected vGAT-IRES-Cre male mice received optical fibers above their nucleus incertus and a multichannel (16 or 32) linear type silicon probe into the dorsal hippocampus. Stainless steel wires above the cerebellum served as reference for the electrophysiological recordings. An additional optical fiber with the tip in the dental acrylate above the skull was used for control illumination sessions. Analgesia was administered during and after the procedures.

Mono-trans-synaptic rabies tracing

We used the monosynaptic rabies tracing technique published by Wickersham et al. (*43*). Briefly, C57Bl/6 and vGAT-Cre mice were prepared for stereotaxic surgeries as described above, and 30 nl of the 1:1 mixture of the following viruses was injected into the NI: AAV2/8-hSyn-FLEX-TVA-p2A-eGFP-p2A-oG and AAV2/5-CAG-FLEX-oG. These viruses contain an upgraded version of the rabies glycoprotein (oG) that has increased trans-synaptic labeling potential (*74*). After 2-3 weeks of survival, mice were injected with the genetically modified Rabies(ΔG)-EnvA-mCherry at the same coordinates. After 10 days of survival, mice were prepared for perfusions.

Antibodies and perfusions

The list and specifications of the primary and secondary antibodies used can be found in Supplementary Table 1-3. Combinations of the used primary and secondary antibodies in the different experiments are listed in

Supplementary Table 4-5. Mice were anesthetized and perfused transcardially with 0.1M phosphate-buffered saline solution for 2 min followed by 4% freshly depolymerized paraformaldehyde solution; or with artificial cerebrospinal fluid (ACSF) for 2 min. After perfusion, brains were removed from the skull, and were immersion-fixed in 4% PFA with or without 0.2% glutaraldehyde (GA) for 2 h. Brains were cut into 50 or 60 µm sections using a vibrating microtome.

Fluorescent immunohistochemistry and laser-scanning confocal microscopy

Perfusion-fixed sections were washed in 0.1 M phosphate buffer (PB) and then incubated in a mixture of primary antibodies for 48-72 h. This was followed by extensive washes in tris buffered saline (TBS), and incubation in the mixture of appropriate secondary antibodies overnight. For visualizing cell layers in the hippocampus, nuclear counterstaining was done on forebrain sections using Draq5 according to the manufacturer`s protocol. Following this, sections were washed in TBS and PB, dried on slides and covered with Aquamount (BDH Chemicals Ltd) or with Fluoromount-G Mounting Medium (Invitrogen). Sections were evaluated using a Nikon A1R confocal laser-scanning microscope system built on a Ti-E inverted microscope operated by NIS-Elements AR 4.3 software. Regions of interests were reconstructed in z-stacks. In case of the monosynaptic rabies tracing experiments, coronal sections were prepared from the whole brain for confocal laser-scanning microscopy, and labeled cells were scanned using a Nikon Ni-E C2+ confocal system.

Immunogold-immunoperoxidase double labeling and electron microscopy

For synaptic detection of $GABA_A$-receptor γ2 subunit, sections were pepsin-treated mildly and were blocked in 1% HSA in TBS, followed by incubation in a mixture of primary antibodies. After washes in TBS, sections were incubated in blocking solution and in mixtures of secondary antibody solutions overnight. After washes in TBS, the sections were treated with 2% glutaraldehyde. The immunoperoxidase reaction was developed using 3-3'-diaminobenzidine as chromogen. Immunogold particles were silver-enhanced. The sections were contrasted using osmium tetroxide solution, dehydrated and embedded in Durcupan. 70-100 nm serial sections were prepared using an ultramicrotome and documented in electron microscope.

Silver-gold intensified and nickel-intensified immunoperoxidase double labeling (SI-DAB/DAB-Ni)

Perfusions, sectioning and incubations of sections in primary antibody solutions were performed as described above. The SI-DAB reaction was followed by subsequent washes and incubation in secondary antibody solutions. Labeling was developed using ammonium nickel sulphate-intensified 3-3'-diaminobenzidine (DAB-Ni) and intensified with silver-gold (SI/DAB) as described in detail in Dobó et al. (*75*). After washes in TBS, sections were blocked in 1% HSA and incubated in primary antibody solutions for the second DAB-Ni reaction. This was followed by incubation with ImmPRESS secondary antibody solutions overnight. The second immunoperoxidase

reaction was developed by DAB-Ni, resulting in a homogenous deposit, which was clearly distinguishable from the silver-gold intensified SI-DAB at the electron microscopic level (*75*). Further dehydration, contrasting and processing of the sections for electron microscopy was performed as described above.

In vitro slice preparation

In all slice studies, brains were removed and placed into an ice-cold cutting solution, which had been bubbled with 95% O_2/5% CO_2 (carbogen gas) for at least 30 min before use. Then 300-450 µm horizontal slices of ventral hippocampi or 300 µm coronal brainstem slices containing the nucleus incertus were cut using a vibrating microtome. After acute slice preparation, slices were placed in an interface-type holding chamber for recovery (*76*). This chamber contained standard artificial cerebrospinal fluid (ACSF) at 35°C that was gradually cooled to room temperature, and saturated with carbogen gas.

Intracellular recordings

To record GABAergic currents, membrane potential was clamped far (~0 mV) from GABA reversal potential. In case of intracellular recordings, fast glutamatergic transmission was blocked by adding the α-amino-3-hydroxy-5-methyl-4-isoxazolepropionic acid (AMPA)-receptor antagonist NBQX and the N-methyl-D-aspartate (NMDA)-receptor antagonist AP-5 to the recording solution. To test $GABA_A$-receptor dependent synaptic transmission, we administered the $GABA_A$-receptor antagonist gabazine into the ACSF. All drugs were administered from stock solutions via pipettes into the ACSF containing superfusion system. For ChR2 illumination, we used a blue laser diode attached to a single optic fiber positioned above the hippocampal slice. For ArchT illumination, we used a red laser diode with optic fiber positioned above NI. Cells recorded in current clamp configuration were depolarized above firing threshold to test the effectivity of ArchT mediated inhibition on action potential generation.

In vivo two-photon calcium imaging

Calcium imaging in head-fixed, behaving mice was performed using a two-photon microscope equipped with an 8 kHZ resonant scanner and a Ti:Sapphire laser tuned to 920 nm. For image acquisition we used a Nikon 40× NIR Apo water-immersion objective (0.8 NA, 3.5 mm WD) coupled to a piezo-electric crystal. Fluorescent signals were collected by a GaAsP photomultiplier tube.

Behavior for two-photon calcium imaging

For the in vivo head-fixed 2P calcium-imaging experiments, behavioral training of the mice was started three days after implantation surgery. Mice were hand habituated, water restricted (>90 % of their pre-deprivation body weight) and trained for 5-7 days to run on a 2 m-long cue-less burlap belt on a treadmill for water rewards, while

being head-fixed. Mice were also habituated to the 2P setup and the scanner and shutter sounds prior to the actual 2P imaging experiments. The treadmill was equipped with a lick-port for water delivery and lick detection. Locomotion was recorded by tracking the rotation of the treadmill wheel using an optical rotary encoder. Stimulus presentation and behavioral read-out were driven by microcontroller systems, using custom made electronics. During random foraging experiments three water rewards were presented per lap in random locations, while mice were running on a cue-less burlap belt. In salience experiments, discrete stimuli were presented as described (*42*), with slight modifications. Stimuli were repeated 10× for each modality in a pseudorandom order during one experiment. The acquired 2P imaging data were pre-processed for further analysis using the SIMA software package (*77*). Motion correction and extraction of dynamic GCaMP6f fluorescent signals were conducted as described (*78*). Regions of interest (ROIs) were drawn manually over the time-averages of motion corrected time-series to isolate the bouton calcium signals of GCaMP6f-expressing axons.

Optogenetics and contextual fear conditioning (CFC)

After optic fiber implantations, mice received 5 days of handling. On the 6th day, mice were placed into the first environmental context (environment "A") in a plexiglass shock chamber, where they received 4 foot-shocks. Optogenetic stimulation was precisely aligned with the shocks, starting 2 seconds before shock onset and finishing 2 seconds after shock offset. For the "ChR2-shifted" group, this laser stimulation was shifted by 15 seconds after shock onset. On the 7th day, mice were placed back into the first environment for 3 minutes to record freezing behavior. This was followed by 5 days of extensive handling to achieve full fear extinction that reset freezing behavior to a normal baseline. On the 13th day, mice were placed into the second environmental context (environment "B"), composed of another set of cues. Baseline freezing levels were recorded for 3 minutes, followed by 4 shocks without optogenetic stimulation. 24 h later, freezing behavior was recorded in the second environment for 3 minutes. The behavior of the mice was recorded and freezing behavior was analyzed manually. Freezing behavior was recorded when mice displayed only respiration-related movements for at least 2 seconds.

Optogenetics and delay cued fear conditioning (CuedFC)

After optic fiber implantations, mice received 5 days of handling. On the 6th day, mice were placed into the first environmental context (environment "A") in a plexiglass shocking chamber, where they received 3 shocks paired with an auditory cue. The footshocks and the auditory cues were co-terminated each time. During the experiment, lasting 6 minutes, mice received a continuous yellow laser light illumination. On the 7th day, mice were placed back into the first environment for 3 minutes to record freezing behavior related to the contextual fear memories. 24 h later, on the 8th day, mice were placed into a second environmental context (environment "B"). Here, mice were presented with the auditory cue for 1 minute to record freezing behavior related to the cued fear memories.

Elevated plus maze (EPM) after optogenetic CFC

One hour after freezing behavior assessment in the first environment (7th day) we placed the mice into an EPM to test their anxiety levels. The cross-shaped EPM apparatus consisted of two open arms with no walls and two closed arms and was on a pedestal 50 cm above floor level (Fig. 6A). The behavior of the mice was recorded camcorder and evaluated using an automated system (Noldus Ethovision 10.0; Noldus Interactive Technologies). Behavior was measured as total time in the open and closed arms.

***In vivo* electrophysiological recordings in freely behaving mice**

Electrophysiological recordings commenced 7-day after surgery and habituation to connections to the head-stage. The signal from the silicon probe was multiplexed and sampled at 20 kHz. The movement of the mouse was tracked by a marker-based, high speed 4-camera motion capture system and reconstructed in 3D. After home cage recording, mice were placed into an open arena and into a linear track. Recordings were repeated 1-7 days later. In each recording situation, blue light stimulation was triggered manually by the experimenter. Mice were recorded in 3 - 9 sessions for 2 - 5 weeks. Then mice were processed for histological verification of the viral transduction zone and implantation. The analysis was performed in MATLAB environment by custom-written functions and scripts. Time-frequency decomposition of pyramidal LFP with continuous wavelet transform (*79*) and subsequent bias correction of spectral power (*80*) was used to calculate instant power.

Data and code availability

Data generated and analysed during the current study are presented in the manuscript or in the Supplementary Materials file, while additional datasets and custom written codes for in vivo electrophysiological recordings, 2P-imaging and data analysis are available from the following links: https://figshare.com/s/9fb345fc23ac2ac94fcd and https://figshare.com/s/5b0c6be2431caf10272b

Figure 1: NI neurons target HIPP SOM-positive neurons with GABAergic synapses

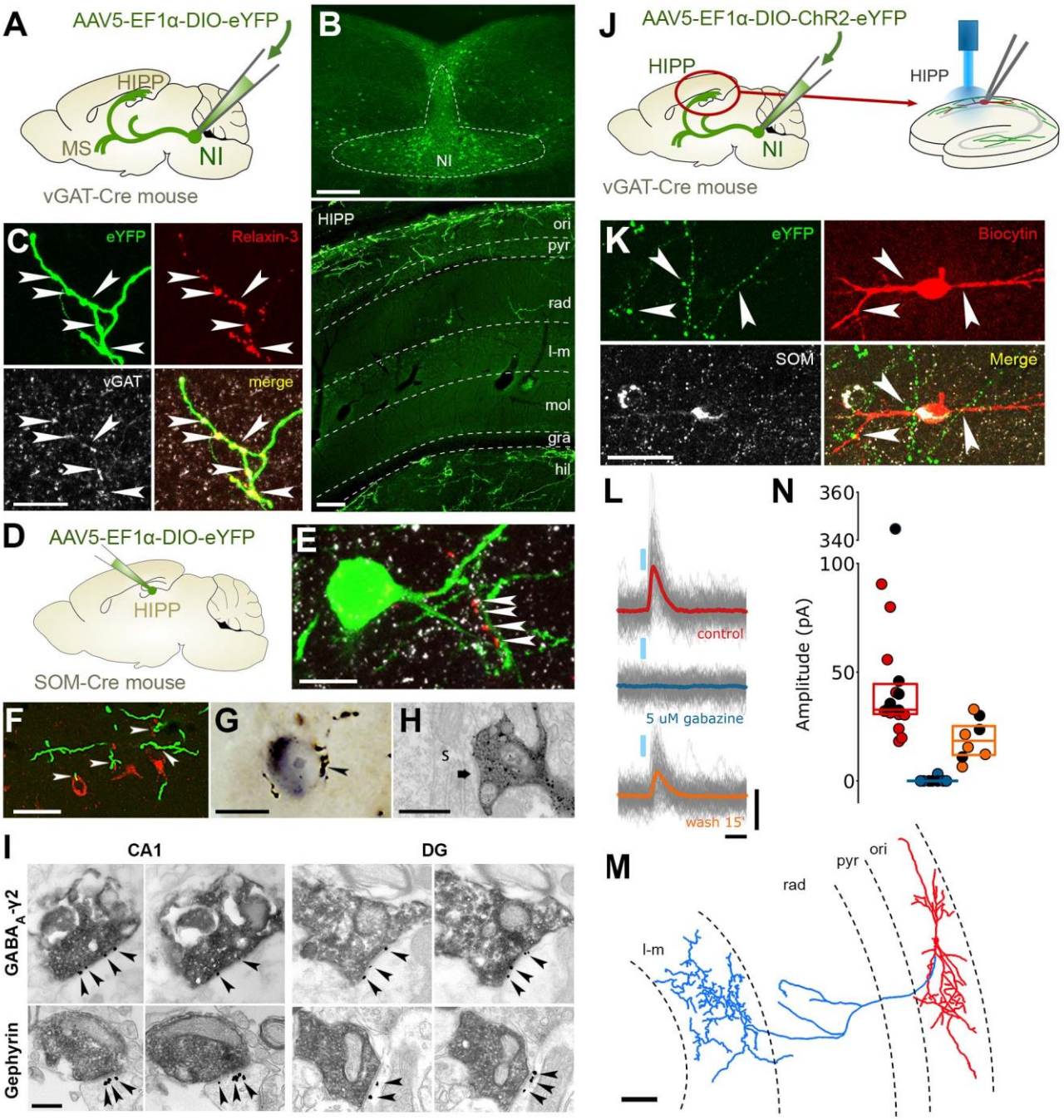

A: AAV2/5-EF1α-DIO-eYFP or AAV2/5-EF1α-DIO-mCherry was injected into the NI of vGAT-Cre mice (n=7). **B**: Images illustrate an injection site (upper panel) and the layer-specific distribution pattern of GABAergic NI fibers in the hippocampus (HIPP) *stratum oriens* and *hilus* (lower panel) where SOM neurons are known to be abundant. Scale bars: 200 µm. **C**: NI fibers (green) in the HIPP are immunopositive for relaxin-3 (red) and vGAT (white). Scale bar: 10 µm. (Also see Suppl. Data for Fig. 1). **D**: AAV2/5-EF1α-DIO-eYFP was injected into the bilateral hippocampus of SOM-Cre mice (n=2). **E**: Relaxin-3 positive NI fibers (red) establish synaptic contacts, marked by gephyrin (white), on SOM-positive interneurons (green) in the HIPP. Scale bar: 10 µm. (Also see Suppl. Data for Fig. 1). **F**: eYFP-positive NI GABAergic fibers (green) in the HIPP establishing putative contacts (white arrowheads) with SOM-positive interneurons (red). Scale bar: 20 µm. **G**: NI GABAergic fiber (labeled with brown silver-gold-intensified-DAB precipitate) establish synaptic contact with a SOM-positive interneuron (labeled with black DAB-Ni precipitate) in the *stratum oriens* of dorsal CA1. Black arrowhead indicates the NI nerve terminal shown in panel G. Scale bar: 10 µm. **H**: The same terminal marked in F establishing a symmetrical synaptic contact (black arrow) on the soma (s) of the SOM-positive interneuron. Scale bar: 600 nm. **I**: EM images of serial sections of AAV-eYFP positive NI terminals (immunperoxidase labeling, black DAB precipitate) that establish symmetrical synaptic contacts in the CA1 *stratum oriens* or in the *hilus (DG)*, containing the $GABA_A$-receptor γ2 subunit (upper row) and the scaffolding protein gephyrin (lower row). The immunogold particles labeling the postsynaptic proteins are marked by black arrowheads. Scale bar: 300 nm. (See Suppl. Data for Fig. 1). **J**: For in vitro recordings AAV2/5-EF1α-DIO-ChR2-eYFP was injected into the NI of vGAT-Cre mice (n=9). After 6 weeks, 300-µm-thick horizontal slices were prepared from the HIPP and transferred into a dual superfusion chamber. Interneurons located in the *stratum oriens* were whole-cell patch clamped in voltage clamp mode, and inhibitory postsynaptic currents (IPSCs) evoked by the optogenetic stimulation of NI GABAergic fibers were measured. (See Supplementary Materials and Methods and Suppl. Data for Fig. 1). **K**: A representative recorded cell (biocytin labeling, red) identified as a SOM-positive interneuron (white). Note the eYFP-positive NI GABAergic fibers (green) with putative contacts targets this neuron (arrowheads). Scale bar: 30 µm. **L**: Optogenetically evoked GABAergic IPSCs of interneuron in panel K. 100 consecutive traces evoked by 2 ms light pulses are overlaid with grey in every conditions. Responses are strong in controls (average in red), but that were completely abolished by 5 µM gabazine (average in blue), and partially recovered after 15 min of washout (average in orange). Scale bars: 10 ms, 40 pA. **M**: Morphological reconstruction of the OLM cell shown in K. Scale bar: 50 µm. **N**: PSC amplitude distribution from all 18 recorded neurons. Identified O-LM cells are filled black dots. (See Suppl. Data for Fig. 1).

Figure 2: NI GABAergic neurons innervate excitatory medial septal neurons and HIPP simultaneously

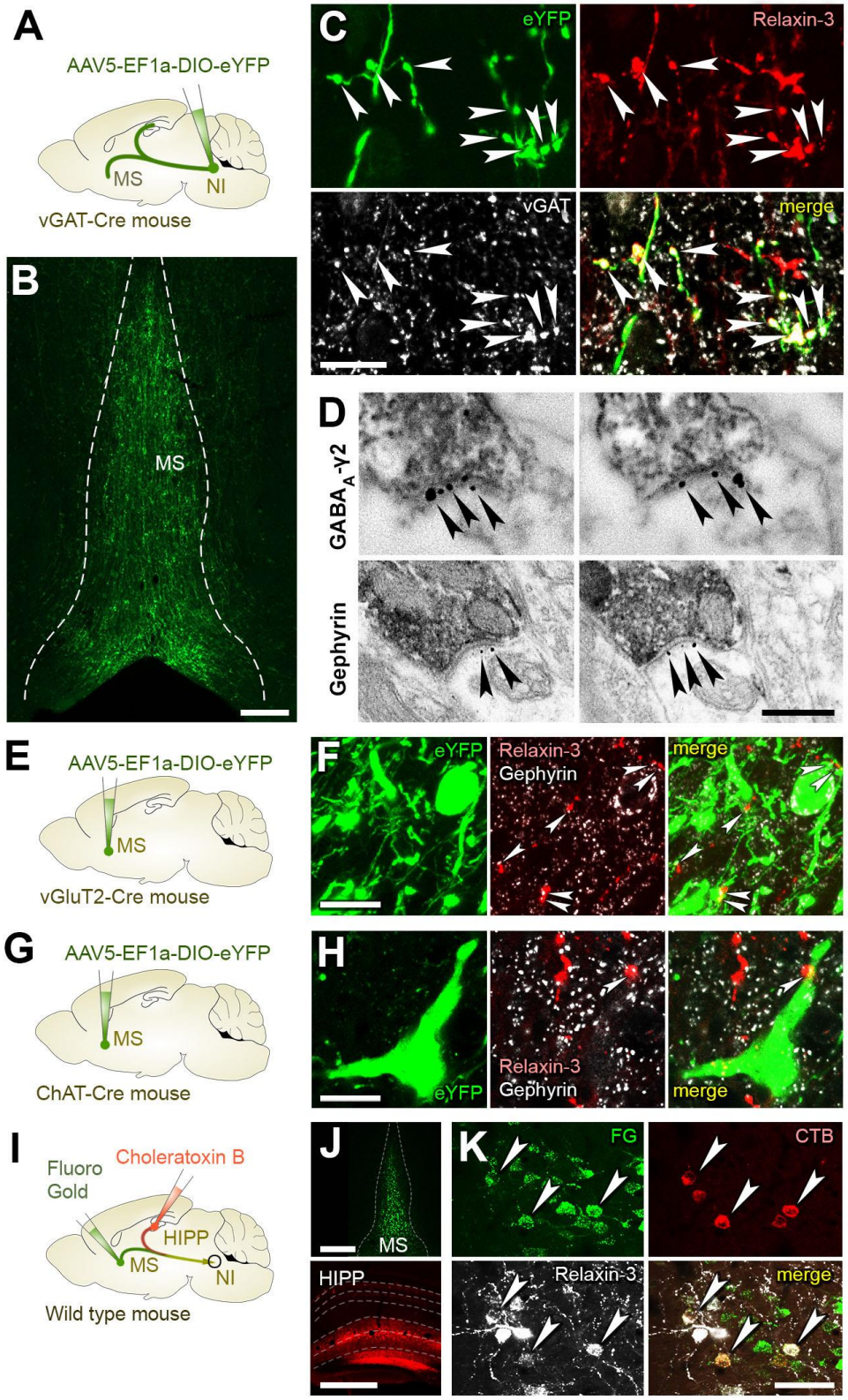

A: AAV2/5-EF1α-DIO-eYFP or AAV2/5-EF1α-DIO-mCherry was injected into the NI of vGAT-Cre mice (n=7).

B: NI GABAergic fibers strongly innervate the medial septum (MS). Scale bar: 200 µm.

C: NI GABAergic fibers in the MS (green) are immunopositive for relaxin-3 (red) and vGAT (white), indicated by white arrowheads. Scale bar: 10 µm. (For statistical data see Suppl. Data for Fig. 2).

D: EM images of serial sections of relaxin-3 positive NI terminals (immunperoxidase labeling, black DAB precipitate) reveal the presence of symmetrical synapses in the MS, containing the $GABA_A$-receptor γ2 subunit (upper row) or the scaffolding protein gephyrin (lower row). The immunogold particles labeling the postsynaptic proteins are marked by black arrowheads. Scale bar: 300 nm. (Suppl. Data for Fig. 2).

E: AAV2/5-EF1α-DIO-eYFP was injected into the NI of vGluT2-Cre mice (n=2).

F: vGluT2-positive neurons (green) are frequently innervated by relaxin-3 positive fibers (red), establishing gephyrin-positive (white) synaptic contacts (white arrowheads) on their dendrites. Scale bar: 10 µm. (See Suppl. Data for Fig. 2). **G**: AAV2/5-EF1α-DIO-eYFP was injected into the NI of ChAT-Cre mice (n=2).

H: ChAT-positive neurons (green) were innervated by relaxin-3 positive fibers (red), establishing gephyrin-positive (white) synaptic contacts (white arrowhead) on their dendrites. Scale bar: 10 µm. (See Suppl. Data for Fig. 2).

I: Double retrograde tracing using FG in the MS and CTB in the bilateral hippocampi, respectively, in wild-type mice (n=3).

J: Representative injection sites revealing green FG labeling in the MS and red CTB labeling in the hippocampus, respectively. The border of the MS and the hippocampal layers are labeled with white dashed lines. Scale bars: 500 µm.

K: Dual projecting neurons containing FG labeling (green) and CTB labeling (red) were frequently detected in the NI, the majority of which were relaxin-3 positive (white neurons, indicated by white arrowheads). Although retrograde tracers cannot fill the entire HIPP or MS, at least 50/135 HIPP-projecting neurons also projected to the MS, and the majority of these neurons (at least 34/50) was positive for relaxin-3. Scale bar: 50 µm.

Figure 3: NI fibers are activated by relevant sensory stimuli in vivo

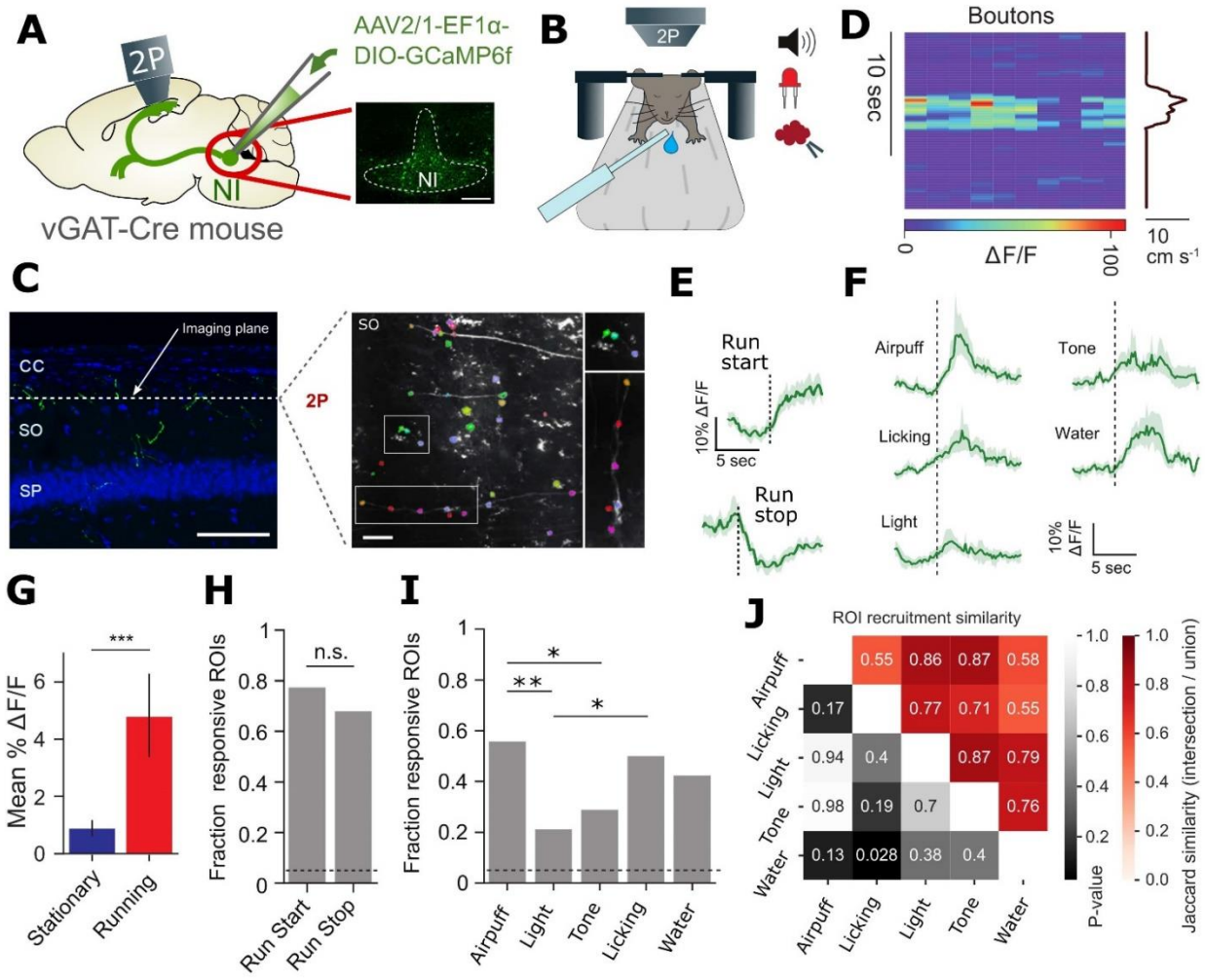

A: Experimental design of the in vivo 2P calcium-imaging experiments. AAV2/1-EF1a-DIO-GCaMP6f was injected into the NI of vGAT-Cre mice (n=5). After recovery, a cranial window implant was placed over the HIPP, and 2P imaging was performed. The inset on the right illustrates a representative virus injection site in the NI. Scale bar: 200 μm.

B: Schematic of 2P imaging and behavioral apparatus. Mice were head-fixed under a 2P microscope on a linear treadmill and permitted to move freely during random foraging experiments. During salience experiments, mice were immobilized and randomly presented with sensory stimuli (water, airpuffs, auditory tone, and light).

C: Left: laser scanning confocal microscopic image of GCaMP6f expressing fibers (green) along with cell nuclei (blue) in the dorsal CA1 region of the HIPP. Scale bar: 100 μm. CC: corpus callosum, SO: *stratum oriens*, SP: *stratum pyramidale*. Right: 2P field of view of GCaMP6f expressing NI GABAergic axons in hippocampal CA1. Exemplary fibers with regions of interest (colored polygons around axonal boutons) are enlarged on the right. Scale bar: 20 μm.

D: A representative random foraging experiment. Left: Fluorescence calcium signal in NI GABAergic axonal boutons; right: animal velocity. **E**: Running event-triggered signal averages during random foraging experiments (grand mean of ROIs + 99% CI, for ROIs with significant responses to each event, bootstrap test, n=3 mice).

F: Signal averages triggered by delivery of sensory stimuli during movement-restrained salience experiments (grand mean of ROIs + 99% CI, for ROIs with significant responses to each stimulus, bootstrap test, n=3 mice).

G: Average fluorescence during stationary and running periods differed significantly. We measured 54 responsive boutons (***: $p<0.001$, Wilcoxon signed-rank test). **H**: Fraction of ROIs responsive to the onset and offset of running. Dashed line indicates the 0.05 chance level of the PETH bootstrap test. There was no statistically significant difference between the two data groups (n.s.: non-significant, $p>0.05$, Z-test). **I**: Fraction of ROIs responsive to sensory stimuli. Dashed line indicates the 0.05 chance level of the PSTH bootstrap test. Light stimuli recruited significantly fewer boutons than licking and air-puff, and auditory tones also recruited a smaller fraction of boutons compared to air-puff (*: $p < 0.05$, **: $p <0.01$ ***: $p<0.001$, Z-test between groups, Bonferroni-corrected p-value).

J: Measure of overlap between the set of ROIs with significant responses to each stimulus (Jaccard similarity values indicated in red boxes). Differences among the fractions of responding ROIs depending on different stimuli was tested using permutation test (p-values indicated in grayscale-colored boxes).

Figure 4: NI receives monosynaptic input from brain areas processing salient environmental stimuli

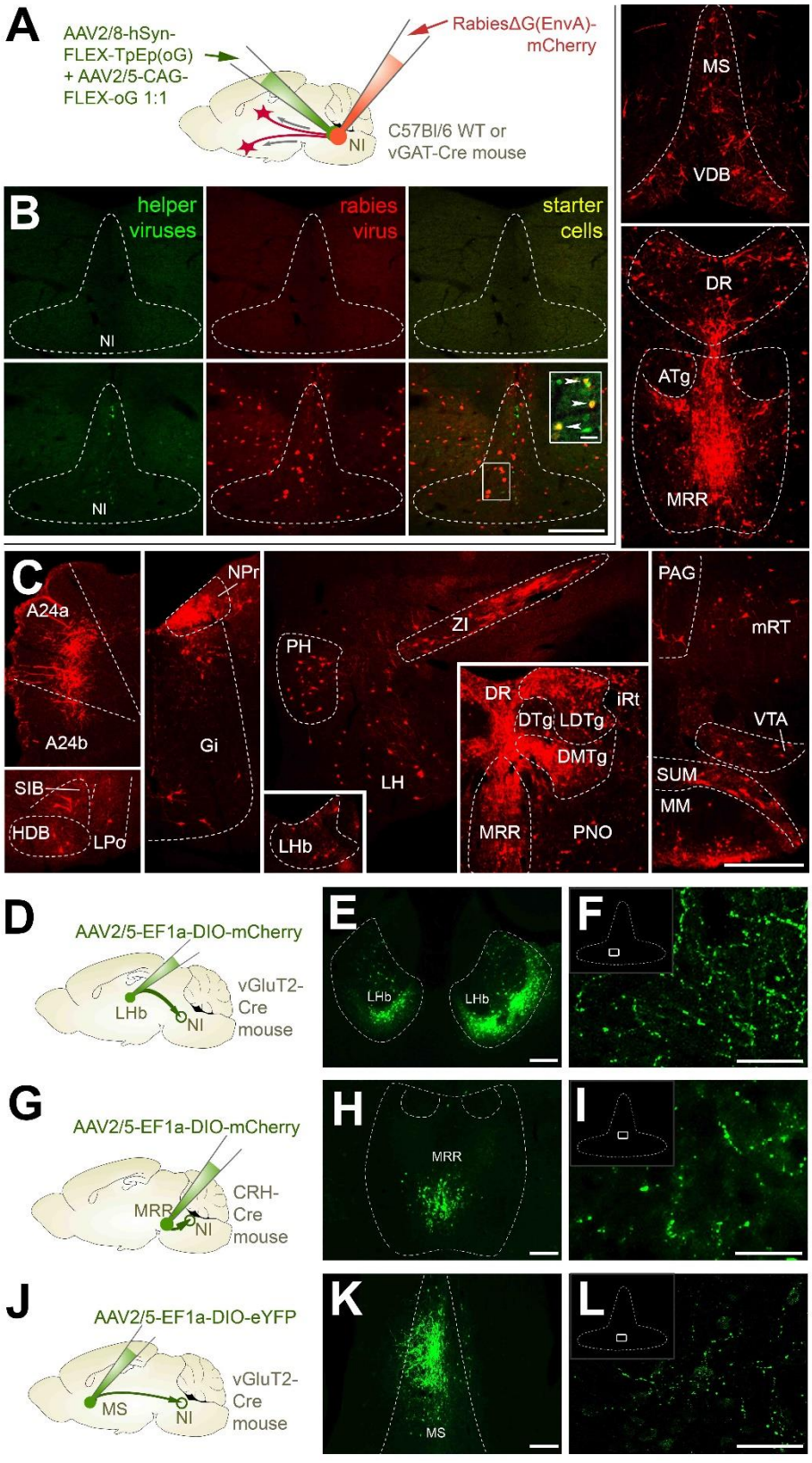

A: A cocktail of helper viruses (AAV2/8-hSyn-FLEX-TpEp(oG) + AAV2/5-CAG-FLEX-oG in a ratio 1:1) was injected into the NI of vGAT-Cre (n=3) or C57Bl/6 WT (n=2) mice, followed by an injection of RabiesΔG(EnvA)-mCherry 2 weeks later.

B: Representative injection sites show the lack of virus expression in WT mice, while there is a strong helper (green) and rabies (red) virus expression present in the NI of vGAT-Cre mice. Inset illustrates some starter neurons expressing both viruses, indicated by white arrowheads. Scale bar for large images: 200 µm. Scale bar for inset: 20 µm.

C: Confocal images illustrate neurons in different brain areas that establish synapses on NI GABAergic neurons. (For abbreviations see Suppl. Data for Fig. 4).

D: AAV2/5-EF1α-DIO-mCherry was injected into the LHb of vGluT2-Cre mice (n=2).

E: A representative injection site reveals mCherry-expression in the vGluT2-positive neurons of the bilateral LHb. Visualized in green for better visibility. Scale bar: 200 µm.

F: Fibers of LHb vGluT2-positive cells heavily innervate NI. Scale bar: 100 µm.

G: AAV2/5-EF1α-DIO-mCherry was injected into the MRR of CRH-Cre mice (n=3).

H: A representative injection site illustrates mCherry-expression in the CRH-positive neurons of the MRR. Visualized in green for better visibility. Scale bar: 200 µm.

I: Fibers of MRR CRH-positive neurons heavily innervate NI. Scale bar: 100 µm.

J: AAV2/5-EF1α-DIO-eYFP was injected into the MS of vGluT2-Cre mice (n=2).

K: A representative injection site reveals eYFP-expression in the vGluT2-positive neurons of the MS. Scale bar: 200 µm.

L: Fibers of MS vGluT2-positive neurons heavily innervate NI. Scale bar: 100 µm.

Figure 5: NI regulates HIPP network activity

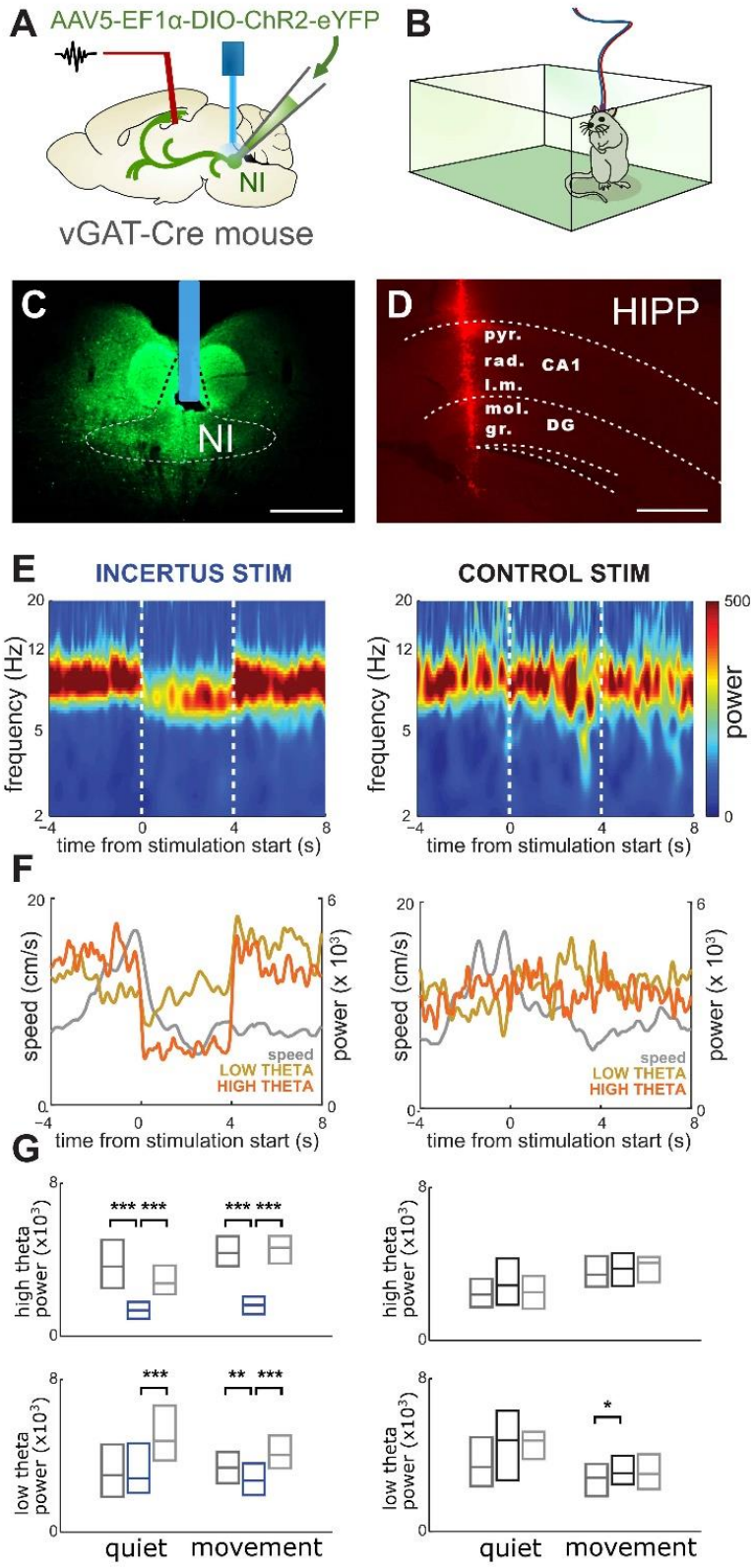

A: Experimental design of optogenetic in vivo experiments in freely-moving mice. AAV2/5-EF1α-DIO-ChR2-eYFP was injected into the NI of vGAT-Cre mice (n=5), and an optic fiber was implanted over the NI, with a linear probe implanted into the dorsal CA1.

B: Five (5) days later, mice were placed into an open field, and their behavior was monitored under freely-moving conditions. NI was stimulated with blue laser pulses, and concurrent hippocampal network activity was recorded.

C: A representative injection site illustrating AAV2/5-EF1a-DIO-ChR2-eYFP (ChR2) expression (green) and the position of the implanted optic fiber (blue) in the NI of a vGAT-Cre mouse. Scale bar: 500 μm.

D: A representative coronal section from the dorsal HIPP CA1 and dentate gyrus (DG) regions illustrating the location of the linear probe. Scale bars: 500 μm.

E: Theta power was reduced by optogenetic stimulation of NI GABAergic cells in ChR2-expressing mice, as revealed by the time-frequency decomposition of pyramidal LFP with continuous wavelet transform. Frequency range of 1-20 Hz is shown, for expanded scale, see Fig. S5C. Averages of all NI GABAergic neurons (left) and control (right) stimulation sessions in one representative mouse during running are shown. Boundaries of the stimulation periods are marked with white dashed lines.

F: Separate analysis of NI stimulation on low theta (5-8 Hz, yellow graph) and high theta (8-12 Hz, orange graph) band power with concurrent speed (grey graph). NI GABAergic cell stimulation was controlled manually, while mice were running on a linear track, and tests started when mice started to demonstrate active exploratory behaviour. NI stimulation strongly reduced high theta band power and also moderately reduced low theta band power, independently from the speed of the animal (left). This effect was absent in control stimulations (left). The mean of all stimulation sessions in 4 mice are shown.

G: High (top) and low (bottom) theta power during quiet (speed < 4 cm/s) and movement (speed > 4 cm/s) periods of stimulation sessions. Theta power during 4s stimulation versus 4s pre- and post-stimulation segments was compared. Medians and interquartile ranges are shown. The instant power values were averaged per stimulation sessions. Statistical difference between the segments was tested by two-sided Wilcoxon signed-rank test (*: $p<0.05$, **: $p<0.01$, ***: $p<0.001$).

Figure 6: NI regulates the establishment of contextual fear memories

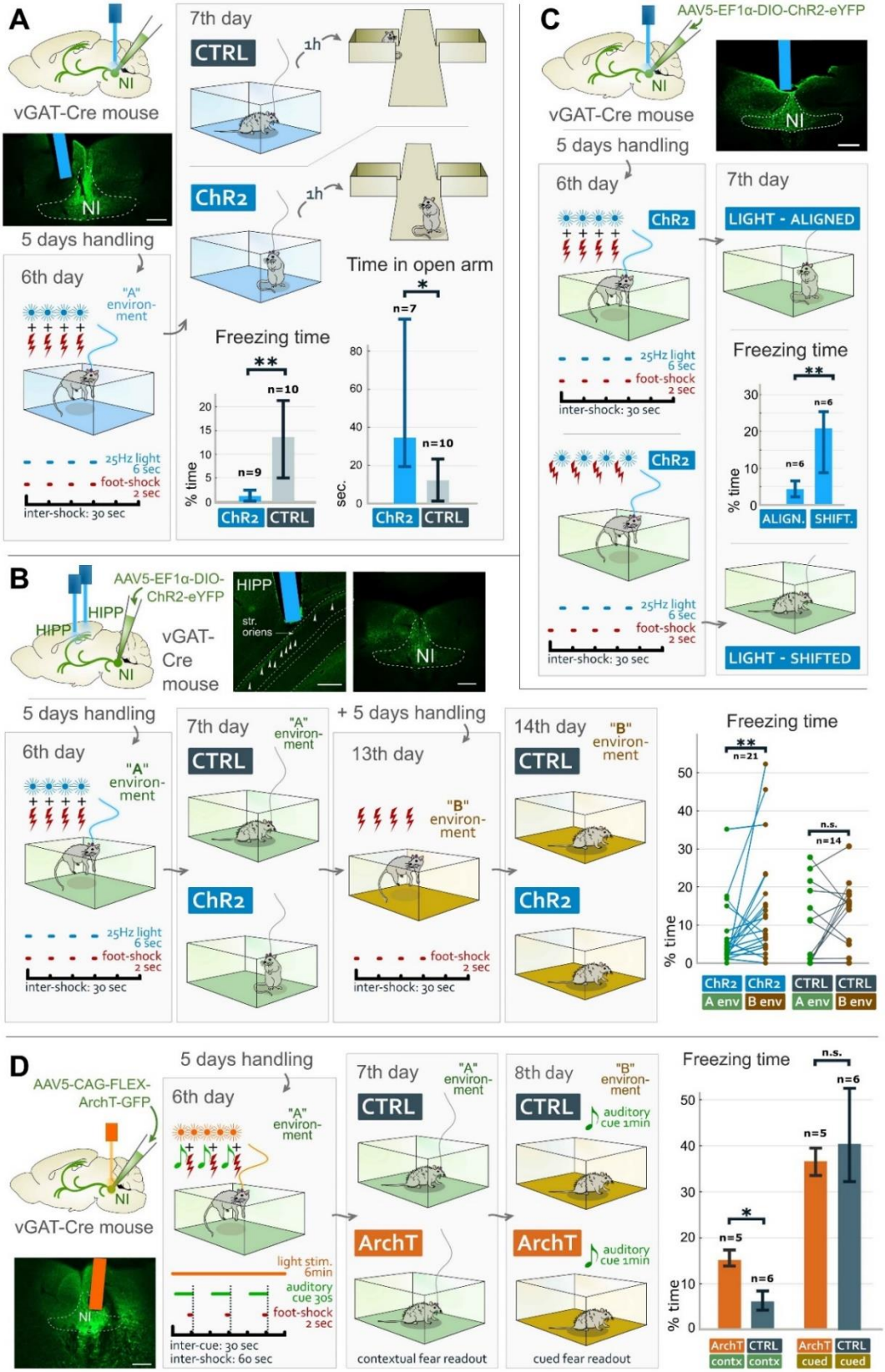

A: Experimental design of contextual fear conditioning experiments with optogenetic stimulation of NI GABAergic neurons. ChR2 expressing mice spent significantly less time freezing in the environment ”A” and significantly more time in the open arm of the elevated plus maze than CTRL mice. Confocal image represents one of the injection sites to label NI GABAergic neurons and the blue area represents the position of the optic fiber. Scale bar: 200 µm. Medians and interquartile ranges are shown on the graphs. (For statistical details see Suppl. Data for Fig. 6).

B: Experimental design of contextual fear conditioning experiments with light stimulation of NI GABAergic fibers in the bilateral HIPP. Illustration of the two sets of experiments in environment “A” and “B” with and without light stimulation of the HIPP fibers of NI GABAergic neurons. Pairwise comparison reveals that ChR2 expressing mice displayed significantly more freezing in environment ”B”, where they received no light stimulation, than in environment ”A”. This was not observed in CTRL mice. Insets illustrate a representative injection site and optic fiber localization; white arrowheads mark NI GABAergic fibers in the HIPP *stratum oriens*. Scale bars: 200 µm. Data from individual mice are shown in the graphs. (For statistical details see Suppl. Data for Fig. 6).

C: Experimental design of contextual fear conditioning experiments with optogenetic stimulation of NI GABAergic neurons “aligned” to or 15 seconds “shifted” after foot-shocks. “Light-aligned” mice displayed significantly less freezing than “Light-shifted” mice, demonstrating the importance of timing. The inset illustrates a representative injection site and optic fiber localization. Scale bar: 200 µm. Medians and interquartile ranges are shown on the graphs. (For statistical details see Suppl. Data for Fig. 6).

D: Experimental design of delayed cued fear conditioning experiments with optogenetic inhibition of NI GABAergic neurons. Light inhibition of NI GABAergic neurons caused significantly stronger contextual freezing behavior in ArchT-mice in environment ”A” compared to CTRL mice. However, there was no difference in HIPP-independent cued fear freezing levels between the two groups in environment ”B”. The inset illustrates a representative injection site and optic fiber localization. Scale bar: 200 µm. Medians and interquartile ranges are shown on the graphs. (For statistical details see Suppl. Data for Fig. 6).

Acknowledgements:

We thank Dr Thomas Reardon (CTRL-Labs, NY) for the AAV2/1-EF1a-DIO-GCaMP6f virus (*16*) used in this study and Dr Darcy S. Peterka and Luke Hammond (ZI Cellular Imaging, CU, New York) for providing microscopy support. We thank Dr Dóra Zelena for her help with CRH-Cre mice. We thank Dr Sébastien Arthaud (INSERM, Lyon, France) for his help with vGluT2-Cre mice. We thank Prof Hanns Ulrich Zeilhofer (UZ, Zürich) for his help with GlyT2-IRES-Cre mice. We thank Prof Josh Huang (CSHL, New York) for his help with SOM-IRES-Cre mice. Viruses used in this study are subject to a material transfer agreement. We thank Dr. László Barna, the Nikon Microscopy Center at IEM, Nikon Austria GmbH and Auro-Science Consulting Ltd. for technical support for fluorescent imaging. We thank Dr. Kornél Demeter and the Behavior Studies Unit of the IEM-HAS for the support for behavioural experiments. We thank Dr. Zsuzsanna Erdélyi and Dr. Ferenc Erdélyi and the staff of the Animal Facility and the Medical Gene Technology Unit of the IEM-HAS for their expert technical help with the breeding and genotyping of the several mouse strains used in this study. We thank Zsuzsanna Bardóczi, Zsuzsanna Hajós, Emőke Szépné Simon, Katalin Lengyel, Márton Mayer, Nándor Kriczky for their help with experiments and Andrea Kriczky, Katalin Iványi and Győző Goda for other assistance.

Funding:

This work was supported by the European Research Council (ERC-2011-ADG-294313, SERRACO), the National Research, Development and Innovation Office, Hungary (OTKA K119521, OTKA K115441, OTKA K109790, OTKA KH124345 and VKSZ_14-1-2O15-0155), the National Institutes of Health, USA (NS030549), the Human Brain Project, EU (EU H2020 720270) and the Hungarian Brain Research Program (2017-1.2.1-NKP-2017-00002). B.P. is supported by UNKP-16-2-13 and D.S. is supported by the UNKP-16-3-IV New National Excellence Program of the Ministry of Human Capacities, Hungary. A.S was supported by the ÚNKP-17-3-III-SE-9 New National Excellence Program of the Ministry of Human Capacities. A.L. is supported by NIMH 1R01MH100631, 1U19NS104590, 1R01NS094668, and the Zegar Family Foundation Award.

Author contributions:

Conceptualization, A.S., G.N.; Investigation, A.S., K.E.S., R.N., D.S., A.D., V.T.T., B.P., P.H., J.P.; Essential reagents: A.L.G., Writing - original draft, A.S., G.N.; Writing - editing, A.S., A.L.G., A.I.G, V.V., A.L., T.F.F., G.N.; Funding acquisition and supervision: A.I.G., V.V., A.L., T.F.F., G.N.

Competing interests:

Authors have no competing interests.

Data and materials availability:

Viruses AAV2/5-EF1α-DIO-eYFP, AAV2/5-EF1α-DIO-mCherry, AAV2/5-CAG-FLEX-ArchT-GFP were obtained under an MTA with the UNC Vector Core. Virus AAV2/5-EF1α-DIO-hChR2(H134R)-eYFP was obtained under an MTA with the Penn Vector Core. Viruses AAV2/8-hSyn-FLEX-TVA-p2A-eGFP-p2A-oG, AAV2/5-CAG-FLEX-

oG, Rabies(ΔG)-EnvA-mCherry were obtained under an MTA with the Salk GT3 Vector Core. The GlyT2-iRES-Cre mouse strain was obtained under an MTA with the University of Zürich.

Supplementary materials contain:

Supplementary Materials and Methods,

Supplementary Text for Main Fig. 1-6,

Figs. S1 to S6,

Tables S1 to S8

References:

1. H. B. Eichenbaum, The hippocampus and declarative memory: cognitive mechanisms and neural codes. *Behav. Brain Res.* **127**, 199–207 (2001).
2. Andersen P., *The Hippocampus Book* (Oxford University Press, 2007).
3. J. Haam, J. Zhou, G. Cui, J. L. Yakel, Septal cholinergic neurons gate hippocampal output to entorhinal cortex via oriens lacunosum moleculare interneurons. *Proc. Natl. Acad. Sci.* **115**, 1886–1895 (2018).
4. T. Kitamura *et al.*, Entorhinal cortical ocean cells encode specific contexts and drive context-specific fear memory. *Neuron*. **87**, 1317–1331 (2015).
5. J. E. Lisman, Relating hippocampal circuitry to function: Recall of memory sequences by reciprocal dentate-CA3 interactions. *Neuron*. **22**, 233–242 (1999).
6. J. Suh, A. J. Rivest, T. Nakashiba, T. Tominaga, S. Tonegawa, Entorhinal cortex layer III input to the hippocampus is crucial for temporal association memory. *Science (80-.).* **1415**, 1415–1421 (2013).
7. T. Kitamura *et al.*, Island cells control temporal association memory. *Science (80-.).* **343**, 896–901 (2014).
8. K. C. Bittner *et al.*, Conjunctive input processing drives feature selectivity in hippocampal CA1 neurons. *Nat. Neurosci.* **18**, 1133–1142 (2015).
9. K. C. Bittner, A. D. Milstein, C. Grienberger, S. Romani, J. C. Magee, Behavioral time scale synaptic plasticity underlies CA1 place fields. *Science (80-.).* **357**, 1033–1036 (2017).
10. J. T. Dudman, D. Tsay, S. A. Siegelbaum, A role for synaptic inputs at distal dendrites: instructive signals for hippocampal long-term plasticity. *Neuron*. **56**, 866–879 (2007).
11. D. S. Roy *et al.*, Distinct neural circuits for the formation and retrieval of episodic memories. *Cell*. **170**, 1000–1012.e19 (2017).
12. S. Maren, M. S. Fanselow, Electrolytic lesions of the fimbria/fornix, dorsal hippocampus, or entorhinal cortex produce anterograde deficits in contextual fear conditioning in rats. *Neurobiol. Learn. Mem.* **149**, 142–149 (1997).
13. R. P. Kesner, Behavioral functions of the CA3 subregion of the hippocampus. *Learn. Mem.* **14**, 771–781 (2007).
14. S. Maren, K. L. Phan, I. Liberzon, The contextual brain: implications for fear conditioning, extinction and psychopathology. *Nat. Rev. Neurosci.* **14**, 417–428 (2013).
15. K. Z. Tanaka *et al.*, The hippocampal engram maps experience but not place. *Science (80-.).* **361**, 392–397 (2018).
16. M. Lovett-Barron *et al.*, Dendritic inhibition in the hippocampus supports fear learning. *Science (80-.).* **1**, 857–864 (2014).
17. S. Siwani *et al.*, OLMα2 Cells Bidirectionally Modulate Learning. *Neuron*. **99**, 404–412 (2018).
18. S. Royer *et al.*, Control of timing, rate and bursts of hippocampal place cells by dendritic and somatic inhibition. *Nat. Neurosci.* **15**, 769–775 (2012).
19. S. Nakauchi, R. J. Brennan, J. Boulter, K. Sumikawa, Nicotine gates long-term potentiation in the hippocampal CA1 region via the activation of α2* nicotinic ACh receptors. *Eur. J. Neurosci.* **25**, 2666–2681 (2007).
20. Y. Jia, Y. Yamazaki, S. Nakauchi, K. Sumikawa, α2 Nicotine receptors function as a molecular switch to continuously excite a subset of interneurons in rat hippocampal circuits. *Eur. J. Neurosci.* **29**, 1588–1603 (2009).
21. R. N. Leão *et al.*, OLM interneurons differentially modulate CA3 and entorhinal inputs to hippocampal CA1 neurons. *Nat. Neurosci.* **15**, 1524–1530 (2012).
22. F. Fuhrmann *et al.*, Locomotion, theta oscillations, and the speed-correlated firing of hippocampal neurons are controlled by a medial septal glutamatergic circuit. *Neuron*. **86**, 1253–1264 (2015).
23. B. Hangya, S. P. Ranade, M. Lorenc, A. Kepecs, Central cholinergic neurons are rapidly recruited by reinforcement feedback. *Cell*. **162**, 1155–1168 (2015).
24. D. Justus *et al.*, Glutamatergic synaptic integration of locomotion speed via septoentorhinal projections. *Nat. Publ. Gr.* (2016), doi:10.1038/nn.4447.

25. I. Misane, A. Kruis, A. W. Pieneman, S. O. Ögren, O. Stiedl, GABA-A receptor activation in the CA1 area of the dorsal hippocampus impairs consolidation of conditioned contextual fear in C57BL/6J mice. *Behav. Brain Res.* **238**, 160–169 (2013).
26. M. Goto, L. W. Swanson, N. S. Canteras, Connections of the nucleus incertus. *J. Comp. Neurol.* **438**, 86–122 (2001).
27. S. Ma *et al.*, Relaxin-3 in GABA projection neurons of nucleus incertus suggests widespread influence on forebrain circuits via G-protein-coupled receptor-135 in the rat. *Neuroscience*. **144**, 165–190 (2007).
28. C. M. Smith *et al.*, Distribution of relaxin-3 and RXFP3 within arousal, stress, affective, and cognitive circuits of mouse brain. *J. Comp. Neurol.* **518**, 4016–4045 (2010).
29. M. Tanaka *et al.*, Neurons expressing relaxin 3/INSL 7 in the nucleus incertus respond to stress. *Eur. J. Neurosci.* **21**, 1659–1670 (2005).
30. A. Nuñez, A. Cervera-Ferri, F. Olucha-Bordonau, A. Ruiz-Torner, V. Teruel, Nucleus incertus contribution to hippocampal theta rhythm generation. *Eur. J. Neurosci.* **23**, 2731–2738 (2006).
31. V. Teruel-Martí *et al.*, Anatomical evidence for a ponto-septal pathway via the nucleus incertus in the rat. *Brain Res.* **1218**, 87–96 (2008).
32. S. Ma, A. Blasiak, F. E. Olucha-Bordonau, A. J. M. Verberne, A. L. Gundlach, Heterogeneous responses of nucleus incertus neurons to corticotrophin-releasing factor and coherent activity with hippocampal theta rhythm in the rat. *J. Physiol.* **591**, 3981–4001 (2013).
33. S. Ma *et al.*, Nucleus incertus promotes cortical desynchronization and behavioral arousal. *Brain Struct. Funct.* **222**, 515–537 (2017).
34. C. García-Díaz *et al.*, Nucleus incertus ablation disrupted conspecific recognition and modified immediate early gene expression patterns in 'social brain' circuits of rats. *Behav. Brain Res.* **356**, 332–347 (2019).
35. T. F. Freund, G. Buzsáki, Interneurons of the hippocampus. *Hippocampus*. **6**, 347–470 (1996).
36. Y. Yanovsky, O. A. Sergeeva, T. F. Freund, H. L. Haas, Activation of interneurons at the stratum oriens/alveus border suppresses excitatory transmission to apical dendrites in the CA1 area of the mouse hippocampus. *Neuroscience*. **77**, 87–96 (1997).
37. F. Ferraguti *et al.*, Immunolocalization of metabotropic glutamate receptor 1α (mGluR1α) in distinct classes of interneuron in the CA1 region of the rat hippocampus. *Hippocampus*. **14**, 193–215 (2004).
38. A. I. Gulyás, N. Hájos, I. Katona, T. F. Freund, Interneurons are the local targets of hippocampal inhibitory cells which project to the medial septum. *Eur. J. Neurosci.* **17**, 1861–1872 (2003).
39. S. Jinno *et al.*, Neuronal diversity in GABAergic long-range projections from the hippocampus. *J. Neurosci.* **27**, 8790–804 (2007).
40. M. Haidar *et al.*, Relaxin-3 inputs target hippocampal interneurons and deletion of hilar relaxin-3 receptors in floxed-RXFP3 mice impairs spatial memory. *Hippocampus*. **27**, 529–546 (2017).
41. S. Jinno, T. Kosaka, Cellular architecture of the mouse hippocampus: A quantitative aspect of chemically defined GABAergic neurons with stereology. *Neurosci. Res.* (2006), , doi:10.1016/j.neures.2006.07.007.
42. P. Kaifosh, M. Lovett-Barron, G. F. Turi, T. R. Reardon, A. Losonczy, Septo-hippocampal GABAergic signaling across multiple modalities in awake mice. *Nat. Neurosci.* **16**, 1182–4 (2013).
43. I. R. Wickersham *et al.*, Monosynaptic restriction of transsynaptic tracing from single, genetically targeted neurons. *Neuron*. **53**, 639–647 (2007).
44. O. Hikosaka, The habenula: from stress evasion to value-based decision making. *Nat. Rev. Neurosci.* **11**, 1–23 (2010).
45. A. M. Stamatakis, G. D. Stuber, Activation of lateral habenula inputs to the ventral midbrain promotes behavioral avoidance. *Nat. Neurosci.* **15**, 1105–1107 (2012).
46. F. Darcet *et al.*, Learning and memory impairments in a neuroendocrine mouse model of anxiety/depression. *Front. Behav. Neurosci.* **8**, 1–13 (2014).
47. J. Peng *et al.*, A quantitative analysis of the distribution of CRH neurons in whole mouse brain. *Front. Neuroanat.* **11**, 1–12 (2017).
48. R. W. Stackman, S. J. Cohen, J. C. Lora, L. M. Rios, Temporary inactivation reveals that the CA1 region of the mouse dorsal hippocampus plays an equivalent role in the retrieval of long-term object memory and

spatial memory. *Neurobiol. Learn. Mem.* **133**, 118–128 (2016).
49. G. Buzsáki, E. I. Moser, Memory, navigation and theta rhythm in the hippocampal-entorhinal system. *Nat. Neurosci.* **16**, 130–138 (2013).
50. R. Boyce, S. D. Glasgow, S. Williams, A. Adamantidis, Causal evidence for the role of REM sleep theta rhythm in contextual memory consolidation. *Science (80-.).* **352**, 812 (2016).
51. J. Basu *et al.*, Gating of hippocampal activity, plasticity, and memory by entorhinal cortex long-range inhibition. *Science (80-.).* **351** (2016), doi:10.1126/science.aaa5694.
52. D. C. Drieskens *et al.*, CA1 inactivation impairs episodic-like memory in rats. *Neurobiol. Learn. Mem.* **145**, 28–33 (2017).
53. V. T. Takács, T. F. Freund, A. I. Gulyás, Types and synaptic connections of hippocampal inhibitory neurons reciprocally connected with the medial septum. *Eur. J. Neurosci.* **28**, 148–164 (2008).
54. V. T. Takács *et al.*, Co-transmission of acetylcholine and GABA regulates hippocampal states. *Nat. Commun.* **9** (2018), doi:10.1038/s41467-018-05136-1.
55. C. W. Pereira *et al.*, Electrolytic lesion of the nucleus incertus retards extinction of auditory conditioned fear. *Behav. Brain Res.* **247**, 201–210 (2013).
56. L. C. Lee, R. Rajkumar, G. S. Dawe, Selective lesioning of nucleus incertus with corticotropin releasing factor-saporin conjugate. *Brain Res.* **1543**, 179–190 (2014).
57. G.-W. Zhang *et al.*, Transforming Sensory Cues into Aversive Emotion via Septal-Habenular Pathway. *Neuron*, 1–13 (2018).
58. S. Martínez-Bellver *et al.*, Regular theta-firing neurons in the nucleus incertus during sustained hippocampal activation. *Eur. J. Neurosci.* **41**, 1049–1067 (2015).
59. S. Martínez-Bellver *et al.*, Causal relationships between neurons of the nucleus incertus and the hippocampal theta activity in the rat. *J. Physiol.* **595**, 1775–1792 (2017).
60. Z. Henderson, G. Fiddler, S. Saha, A. Boros, K. Halasy, A parvalbumin-containing, axosomatic synaptic network in the rat medial septum: Relevance to rhythmogenesis. *Eur. J. Neurosci.* **19**, 2753–2768 (2004).
61. A. Joshi, M. Salib, T. J. Viney, D. Dupret, P. Somogyi, Behavior-Dependent Activity and Synaptic Organization of Septo-hippocampal GABAergic Neurons Selectively Targeting the Hippocampal CA3 Area. *Neuron*. **96**, 1342–1357.e5 (2017).
62. G. Gangadharan *et al.*, Medial septal GABAergic projection neurons promote object exploration behavior and type 2 theta rhythm. *Proc. Natl. Acad. Sci. U. S. A.* **113**, 6550–5 (2016).
63. Z. Borhegyi, Phase Segregation of Medial Septal GABAergic Neurons during Hippocampal Theta Activity. *J. Neurosci.* **24**, 8470–8479 (2004).
64. H. Albert-Gascó *et al.*, Central relaxin-3 receptor (RXFP3) activation increases ERK phosphorylation in septal cholinergic neurons and impairs spatial working memory. *Brain Struct. Funct.* **BSAF-D-15-** (2016), doi:10.1007/s00429-016-1227-8.
65. F. E. Olucha-Bordonau *et al.*, Distribution and targets of the relaxin-3 innervation of the septal area in the rat. *J. Comp. Neurol.* **520**, 1903–1939 (2012).
66. A. I. Gulyás, T. J. Görcs, T. F. Freund, Innervation of different peptide-containing neurons in the hippocampus by gabaergic septal afferents. *Neuroscience*. **37**, 31–44 (1990).
67. T. F. Freund, M. Antal, GABA-containing neurons in the septum control inhibitory interneurons in the hippocampus. *Nature*. **336**, 170–3 (1988).
68. B. Hangya, Z. Borhegyi, N. Szilágyi, T. F. Freund, V. Varga, GABAergic neurons of the medial septum lead the hippocampal network during theta activity. *J. Neurosci.* **29**, 8094–8102 (2009).
69. A. Eskildsen, L. P. Andersen, A. D. Pedersen, S. K. Vandborg, J. H. Andersen, Work-related stress is associated with impaired neuropsychological test performance: A clinical cross-sectional study. *Stress*. **18**, 198–207 (2015).
70. E. S. Parker, L. Cahill, J. L. McGaugh, A case of unusual autobiographical remembering. *Neurocase*. **12**, 35–49 (2006).
71. S. Kamiya, Relationship between frequency of involuntary autobiographical memories and cognitive failure. *Memory*. **22**, 839–851 (2014).

72. L. Borgius, C. E. Restrepo, R. N. Leao, N. Saleh, O. Kiehn, A transgenic mouse line for molecular genetic analysis of excitatory glutamatergic neurons. *Mol. Cell. Neurosci.* **45**, 245–257 (2010).
73. K. F. George Paxinos, Paxinos and Franklin's the Mouse Brain in Stereotaxic Coordinates. *São Paulo, Acad. Press* (2012), p. 360 p., (available at https://www.elsevier.com/books/paxinos-and-franklins-the-mouse-brain-in-stereotaxic-coordinates/paxinos/978-0-12-391057-8).
74. E. J. Kim, M. W. Jacobs, T. Ito-Cole, E. M. Callaway, Improved Monosynaptic Neural Circuit Tracing Using Engineered Rabies Virus Glycoproteins. *Cell Rep.* **15**, 692–699 (2016).
75. E. Dobó *et al.*, New silver-gold intensification method of diaminobenzidine for double-labeling immunoelectron microscopy. *J. Histochem. Cytochem.* **59**, 258–269 (2011).
76. N. Hájos *et al.*, Maintaining network activity in submerged hippocampal slices: Importance of oxygen supply. *Eur. J. Neurosci.* **29**, 319–327 (2009).
77. P. Kaifosh, J. D. Zaremba, N. B. Danielson, A. Losonczy, SIMA: Python software for analysis of dynamic fluorescence imaging data. *Front. Neuroinform.* **8**, 1–10 (2014).
78. N. B. B. Danielson *et al.*, Distinct contribution of adult-born hippocampal granule cells to context encoding. *Neuron*. **90**, 101–112 (2016).
79. C. Torrence, G. P. Compo, A Practical Guide to Wavelet Analysis. *Bull. Am. Meteorol. Soc.*, 61–78 (2010).
80. Y. Liu, X. S. Liang, R. H. Weisberg, Rectification of the bias in the wavelet power spectrum. *J. Atmos. Ocean. Technol.* **24**, 2093–2102 (2007).

Supplementary Materials for

Brainstem Nucleus Incertus Controls Contextual Memory Formation

András Szőnyi, Katalin E. Sos, Rita Nyilas, Dániel Schlingloff, Andor Domonkos, Virág. T. Takács, Balázs Pósfai, Panna Hegedüs, James B. Priestley, Andrew L. Gundlach, Attila I. Gulyás, Viktor Varga, Attila Losonczy, Tamás F. Freund and Gábor Nyiri

correspondence to: nyiri.gabor@koki.mta.hu

This PDF file includes:

Supplementary Materials and Methods

Ethical considerations

All experiments were performed in accordance with the Institutional Ethical Codex and the Hungarian Act of Animal Care and Experimentation guidelines (40/2013, II.14), which are in concert with the European Communities Council Directive of September 22, 2010 (2010/63/EU). The Animal Care and Experimentation Committee of the Institute of Experimental Medicine of Hungarian Academy of Sciences and the Animal Health and Food Control Station, Budapest, have also approved the experiments under the project number PE/EA/2553-6/2016. All two-photon (2P) imaging experiments were conducted in accordance with the United States of America, National Institutes of Health guidelines and with the approval of the Columbia University Institutional Animal Care and Use Committee.

Mice

The following mouse strains were used in the experiments: C57Bl/6J wild type, ChAT-iRES-Cre, CRH-iRES-Cre, vGAT-iRES-Cre, vGAT-iRES-Cre::Gt(ROSA26)Sor-CAG/tdTomato (all strains from The Jackson Laboratory), vGluT2-iRES-Cre (received from Dr Sébastien Arthaud) (71), GlyT2-iRES-Cre (courtesy of Prof Hanns Ulrich Zeilhofer) and SOM-iRES-Cre (courtesy of Prof Josh Huang). We used adult (at least 6 weeks-old) mice from both genders in our experiments. Mice had ad libitum access to food and water. Mice were housed in a vivarium (3-5 mice/cage) until used in experiments. Mice used for 2P-experiments were maintained on a reversed 12h light-dark cycle, with experiments performed during the dark phase of the cycle. Mice used for all other experiments were maintained on a normal 12h light-dark cycle, with experiments performed during the light phase of the cycle.

Stereotaxic surgeries for viral gene transfer and retrograde tracing

Mice were anesthetized with 2% isoflurane followed by an intraperitoneal injection of an anesthetic mixture (containing 8.3 mg/ml ketamine and 1.7 mg/ml xylazine-hydrochloride in 0.9% saline, 10 ml/kg body weight); and were then mounted in a small animal stereotaxic frame (David Kopf Instruments, CA, USA) and the skull surface was exposed. A Nanoject II precision microinjector pump (Drummond, Broomall, PA) was used for the microinjections. For 2P-microscopic, anterograde tracing and optogenetic experiments 10-100 nl of one of the following viruses were injected into the target brain areas: AAV2/1-EF1a-DIO-GCaMP6f (courtesy of Dr Thomas Reardon); AAV2/5-EF1α-DIO-eYFP; AAV2/5-EF1α-DIO-mCherry; AAV2/5-CAG-FLEX-ArchT-GFP (UNC Vector Core); AAV2/5-EF1α-DIO-hChR2(H134R)-eYFP (Penn Vector Core; 4.4-8.5×1012 colony forming units/ml for all viruses). For retrograde tracing experiments we injected 20-40 nl of 2% FluoroGold (Fluorochrome, Denver, CO, USA) or 0.5% Cholera toxin B subunit (List Biologicals, Campbell, CA, USA) into the target areas. The coordinates for the injections were defined by a stereotaxic atlas (72); the null coronal plane of the anteroposterior axis was defined by the position of Bregma; the null sagittal plane of the mediolateral axis was defined by the sagittal suture; the null horizontal plane of the dorso-ventral axis was defined by the bregma and lambda. The injection coordinates were the following (always given in mm at the anteroposterior, mediolateral

and dorsoventral axes, respectively): nucleus incertus: -5.0, 0.0, -4.2; hippocampus: (SOM-Cre, 4-4 injections bilaterally) -2.5, +/- 1.5, -2.1 and -1.5; or -2.0, +/-1.3, -2.0 and -1.5; (WT HIPP-HIPP retrograde tracing, 3-3 injections unilaterally per tracer) -2.0, +/-1.5, -1.7; or -2.7, +/-2.2, -1.8; or -3.3, +/-3.0, -2.7; (WT MS-HIPP retrograde tracing, 2-2 injections bilaterally) -2.0, +/-1.5, -1.7; or -3.0, +/-3.0, -3.0; MS: +1.0, 0.0, -4.3; subiculum: -4.2, +/-3.0, and -3.5.

Definition of the area of nucleus incertus

In the brainstem reticular formation, borders of "nuclei" are not well-defined. For instance, NI is best defined by neurons expressing relaxin-3 mRNA/peptide (28, Figure 1). Although relaxin-3 immunostaining is better detected in nerve terminals in the region, relaxin-3 positive neurons are scattered several tens of micrometers outside the NI "borders" defined by the Allen Brain Atlas (28, Figure 1), while dendritic arrays of NI neurons cross all these putative borders as well. However, in mice the NI is still a relatively small area located below the 4th ventricle, occupying about 500 and 1000 μm in antero-posterior and lateral axes, respectively, which functionally belong to the same cell population. Putative borders, defined by the Allen Brain Atlas, indicated here are given only as a reference, because the region is recognized more easily this way.

Hippocampal cranial window implants for two-photon imaging experiments

Mice spent at least 3 days post injection in their home cages to recover, and then were surgically implanted with an imaging window/head-post implant as described (16). Briefly, under isoflurane anesthesia, a 3-mm diameter craniotomy was made in the exposed skull over the left dorsal hippocampus. After gentle removal of the dura, the underlying cortex was slowly aspirated with continuous irrigation with chilled ACSF until fibers of the corpus callosum were exposed. A custom-made sterilized cylindrical steel imaging cannula with a glass cover slip window (3-mm diameter × 1.5-mm height, as described in (41) was inserted into the craniotomy and was cemented to the skull with dental acrylic (Unifast Trad) along with a stainless-steel headpost for head-fixation. Buprenorphine analgesia (0.05-0.1 mg/kg, sc.) was administered during the procedure and for three days after the surgery to minimize post-operative discomfort.

Optic fiber implantations for behavioral experiments

The highly-specific manipulation of GABAergic neurons in the NI area was achieved by the combination of three factors: (1) we infected only GABAergic cells in vGAT-Cre mice, (2) we infected only the area of the NI (which was confirmed anatomically), and (3) optic fibers targeted only the NI or the hippocampus (Fig. S4). The highly restricted infection or specific optic stimulations would have been sufficiently selective individually, but their combination ensures the best possible specificity.

For behavioral experiments, during a second surgical procedure 5-6 weeks after virus injections, optic fibers (105 μm core diameter, 0.22 NA, Thorlabs GmbH, Dachau/Munich, Germany) were implanted into the brain with the tip at the following coordinates: nucleus incertus: -5.0, 0.0, -4.1; hippocampus: -2.5, +/-2.2, -1.7. For secure fixture of the implantable optic fiber, 3 screws were inserted into the skull followed by disinfection and drying the surface with 70% ethanol and finally, dental cement (Paladur, M+W Dental, Hungary) was added between the skull and the base of the ceramic ferrule

of the fiber implant (Precision Fiber Products, CA, USA). Positions of the optic fibers are illustrated in Fig. S4A-B. After the surgeries, mice received 0.5-0.7 ml saline and 0.03-0.05 mg/kg meloxicam (Metacam, Boehringer Ingelheim, Germany) intraperitoneally, and were placed into separate cages until further experiments or perfusions.

Stereotaxic surgeries for electrophysiological recordings in freely moving mice

Anesthesia of AAV2/5-EF1a-DIO-hChR2(H134R)-YFP-WPRE transfected vGAT-IRES-Cre male mice (time interval between virus injection and surgery: 102±42 days) was induced by intraperitoneal injection of ketamine-xylazine (4 to 1) combination diluted (1:6) in Ringer's lactate solution (10 ml/kg body weight) and maintained by isoflurane during head fixation in the stereotaxic frame. After local disinfection by Betadine and local analgesia by 10% lidocaine-spray (both from Egis Pharmaceuticals PLC, Budapest, Hungary), the cranium was exposed and cleaned for application of adhesive agent (OptiBond XTR, Kerr Corporation, Orange, CA). After photocuration, stereotaxically-guided craniotomies were performed for implantation of the optical fiber (105 μm core diameter, 0.22 NA, Thorlabs GmbH, Dachau/Munich, Germany) above the nucleus incertus (-5.4, 0.0 with tip -3.1 mm from the brain surface) and a multichannel (16 or 32) linear type silicon probe (Neuronexus, Ann-Arbor, MI) into the dorsal hippocampus (AP -2.5, +2 with tip -2.1 mm from brain surface). Two additional small holes were drilled above the cerebellum for stainless steel wires serving as ground and reference for the electrophysiological recordings. The optical fiber and a custom-made microdrive holding the silicon probe were fixed to the skull using dental acrylate (Paladur, Heraeus Kulzer GmbH, Hanau, Germany). The craniotomy above the hippocampus was sealed with artificial dura (Cambridge NeuroTech Ltd, Cambridge, UK). The probe-microdrive assembly was shielded by a copper mesh preventing the contamination of the recordings by environmental electric noise. The mesh was also covered by dental acrylate. An additional optical fiber with the tip limited to the dental acrylate above the skull was used for control illumination sessions. Before finishing the surgery, buprenorphine (0.045 mg/kg body weight) was subcutaneously injected. Following all surgeries, the mice were continuously monitored until recovered as demonstrated by their ability to exhibit purposeful movements.

Mono-trans-synaptic rabies tracing

A detailed description of the monosynaptic rabies tracing technique used has already been published by Wickersham et al. (42). Briefly, C57Bl/6 and vGAT-Cre mice were prepared for stereotaxic surgeries as described above, and 30 nl of the 1:1 mixture of the following viruses was injected into the NI at the coordinates given above: AAV2/8-hSyn-FLEX-TVA-p2A-eGFP-p2A-oG and AAV2/5-CAG-FLEX-oG (4.5×1012 colony forming units/ml). These viruses contain an upgraded version of the rabies glycoprotein (oG) that has increased trans-synaptic labeling potential (73). After 2-3 weeks of survival, mice were injected with the genetically modified Rabies(ΔG)-EnvA-mCherry (3.5×107 colony forming units/ml) at the same coordinates. After 10 days of survival, mice were prepared for perfusions. Cells can be the initiators of transsynaptic spread (starter cells) only if they contain both helper viruses (green color) and the rabies viruses (red color). We used only those mice, in which starter cells could be found strictly in the area of NI only, therefore the transsynaptic spread from the surrounding areas could be excluded, as

illustrated in the representative image of Figure 4B. Theoretically, in the area of the helper virus injection site, trans-synaptic jumps are possible between cells that are interconnected and express the G-protein. It is unknown if these jumps would be able to create an efficient starter cell. However, the helper virus injection site is confined to the NI area and infected cells can be only GABAergic neurons, because the G-protein expressing helper virus is also Cre-dependent. Therefore, initial trans-synaptic jumps are theoretically possible only within the area of NI, and it may even be beneficial for slightly amplifying starter cell number within NI, however frequently or otherwise it occurs.

Antibodies

The list and specifications of the primary and secondary antibodies used can be found in Supp. Table 1-3. The specificities of the primary antibodies were extensively tested, using knock-out mice if possible. Secondary antibodies were extensively tested for possible cross-reactivity with the other antibodies used, and possible tissue labeling without primary antibodies was also tested to exclude auto-fluorescence or specific background labeling. No specific-like staining was observed under these control conditions. Combinations of the used primary and secondary antibodies in the different experiments are listed in Supp. Table 4-5.

Perfusions

Mice used in 2P imaging experiments were deeply anaesthetized with 2% isoflurane. Mice used in all other experiments were anesthetized with 2% isoflurane followed by an intraperitoneal injection of an anesthetic mixture (containing 8.3 mg/ml ketamine, 1.7 mg/ml xylazine-hydrochloride, 0.8 mg/ml promethazinium-chloride) to achieve deep anesthesia. The mice were then perfused transcardially (protocol A) with 0.1M phosphate-buffered saline (PBS, pH 7.4) solution for 2 min followed by 30 ml of 4% freshly depolymerized paraformaldehyde (PFA) solution; (protocol B) with PBS for 2 min, followed by PFA for 40 min, followed by PBS for 10 min; (protocol C) with artificial cerebrospinal fluid (ACSF) for 2 min containing the following reagents (in mM): 125.0 NaCl, 2.5 KCl, 25.0 glucose, 1.25 NaH_2PO_4, 2.5 $CaCl_2$-$2H_2O$, 2 $MgCl_2$-$6H_2O$ and 26 $NaHCO_3$. All salts were obtained from Sigma-Aldrich. After perfusion, brains were removed from the skull, and brains perfused using protocols A and B were immersion-fixed in 4% PFA with or without 0.2% glutaraldehyde (GA) for 2 h. Brains were cut into 50 or 60 μm sections using a vibrating microtome (Leica VT1200S or Vibratome 3000).

Fluorescent immunohistochemistry and laser-scanning confocal microscopy

Perfusion-fixed sections were washed in 0.1 M phosphate buffer (PB, pH 7.4), and incubated in 30% sucrose overnight for cryoprotection. Sections were then freeze-thawed over liquid nitrogen three times for antigen retrieval. Sections were subsequently washed in PB and Tris-buffered saline (TBS, pH 7.4) and blocked in 1% human serum albumin in TBS (HSA; Sigma-Aldrich) and then incubated in a mixture of primary antibodies for 48-72 h. This was followed by extensive washes in TBS, and incubation in the mixture of appropriate secondary antibodies overnight. For visualizing cell layers in the hippocampus, nuclear counterstaining was done on forebrain sections using Draq5

(1:1000, Biostatus) according to the manufacturer`s protocol. Following this, sections were subsequently washed in TBS and PB, dried on slides and covered with Aquamount (BDH Chemicals Ltd) or with Fluoromount-G Mounting Medium (Invitrogen). For the viral injection and retrograde tracing experiments, each injection site was reconstructed from 50 µm sections using a Zeiss Axioplan2 microscope. For the retrograde tracing experiments, we also estimated what percentage of the injected brain area was labeled with the tracer. Every part of the injected tissue containing even low levels of tracer was considered as part of the injection site. We fitted every image of the injection sites to the corresponding outlines of the atlas (72), and determined the ratio of the volumes of the injection sites to the injected brain area, using the Fiji/ImageJ software. The brain areas measured were the following based on the atlas: in the hippocampus, the dentate gyrus and the regions CA1-3; in the MS, the medial septal area and the vertical diagonal band of Broca. Sections were evaluated using a Nikon A1R confocal laser-scanning microscope system built on a Ti-E inverted microscope with a 10× air objective or with a 0.45 NA CFI Super Plan Fluor ELWD 20XC or with a 1.4 NA CFI Plan Apo VC 60× oil objective or with a Nikon Ni-E C2+ confocal system equipped with a 0.75 NA Plan Apo VC DIC 20× objective, both operated by NIS-Elements AR 4.3 software. Regions of interests were reconstructed in z-stacks; distance between the focal planes was 0.5 µm for examined synaptic contacts and 2 µm for examined neuronal somata.

In case of the monosynaptic rabies tracing experiments, coronal sections spaced at 300 µm were prepared from the whole brain for confocal laser-scanning microscopy, and every transsynaptically labeled cell was scanned using a Nikon Ni-E C2+ confocal system equipped with a 0.13 NA Plan Fluor 4× objective operated by NIS-Elements AR 4.3 software. The cell counting was performed using the Adobe Photoshop CS6 software.

Immunogold-immunoperoxidase double labeling and electron microscopy

Perfusion-fixed sections were washed in 0.1 M phosphate buffer (PB) for 1 hour, then cryoprotected by incubation in 30% sucrose overnight and freeze-thawed three times over liquid nitrogen. For synaptic detection of gephyrin, sections were washed in 0.1 M PB and in TBS and blocked in 1% human serum albumin in TBS (HSA; Sigma-Aldrich), followed by incubation in a mixture of primary antibodies for 48-72 h. For synaptic detection of GABAA-receptor γ2 subunit, sections were pretreated with 0.2 M HCl solution containing 2 mg/ml pepsin (Dako) at 37°C for 8 min. Then sections were blocked in 1% HSA in TBS, followed by incubation in a mixture of primary antibodies. After repeated washes in TBS, sections were incubated in blocking solution (Gel-BS) containing 0.2% cold water fish skin gelatin (Aurion) and 0.5% HSA in TBS for 1 h. Sections were then incubated in mixtures of secondary antibody solutions overnight. After intensive washes in TBS, the sections were treated with 2% glutaraldehyde in 0.1 M PB for 15 min to fix the gold particles in the tissue. To develop the labeling for NI fibers, this was followed by incubation in avidin-biotinylated horseradish peroxidase complex (Elite ABC; 1:300; Vector Laboratories) diluted in TBS for 3 h. The immunoperoxidase reaction was developed using 3-3′-diaminobenzidine (DAB; Sigma-Aldrich) as chromogen. To enlarge immunogold particles, this was followed by incubation in silver enhancement solution (SE-EM; Aurion) for 40-70 min at room temperature. The sections were treated with 0.5% osmium tetroxide in 0.1 M PB on ice and they were dehydrated in ascending alcohol series and in acetonitrile and embedded in

Durcupan (ACM; Fluka). During dehydration, the sections were treated with 1% uranyl-acetate in 70% ethanol for 20 min. After this, 70-100 nm serial sections were prepared using an ultramicrotome (Leica EM UC6) and collected on single-slot copper grids. Sections were examined using a Hitachi H-7100 electron microscope and a Veleta CCD camera driven by the iTEM 5.0 software (Olympus). Randomly sampled terminals of the NI establishing synaptic contacts in the HIPP and MS were always fully reconstructed.

Silver-gold intensified and nickel-intensified immunoperoxidase double labeling (SI-DAB/DAB-Ni)

Perfusions, sectioning and incubations of sections in primary antibody solutions were performed as described. The SI-DAB reaction was followed by subsequent washes in the appropriate secondary antibody solutions for 24h in TBS. After subsequent washes in TBS and incubation in avidin-biotin-peroxidase complex for 3 h (ABC Elite 1:300, Vector Laboratories), ammonium nickel sulphate-intensified 3-3'-diaminobenzidine (DAB-Ni) was used for the development of immunoperoxidase reaction. This reaction was further intensified with silver-gold (SI/DAB) as described in detail in Dobó et al. (74). This intensification step converts the labeling from homogenous to granular by loading fine gold particles onto the DAB-Ni deposit. After washes in TBS, sections were blocked in 1% HSA for 1 h and incubated in primary antibody solutions for the second DAB-Ni reaction for 48-72 h. This step was followed by incubation with ImmPRESS secondary antibody solutions overnight. The second immunoperoxidase reaction was developed by DAB-Ni, resulting in a homogenous deposit, which was clearly distinguishable from the silver-gold intensified SI-DAB at the electron microscopic level (74). Further dehydration, contrasting and processing of the sections for electron microscopy was performed as described above.

In vitro slice preparation

In all slice studies, mice were decapitated under deep isoflurane anesthesia. The brain was removed and placed into an ice-cold cutting solution, which had been bubbled with 95% O2/5% CO2 (carbogen gas) for at least 30 min before use. The cutting solution contained the following (in mM): 205 sucrose, 2.5 KCl, 26 NaHCO3, 0.5 CaCl2, 5 MgCl2, 1.25 NaH2PO4, 10 glucose. After this, 300-450 µm horizontal slices of ventral hippocampi or 300 µm coronal brainstem slices containing the nucleus incertus were cut using a Vibratome (Leica VT1000S). After acute slice preparation, slices were placed in an interface-type holding chamber for recovery. This chamber contained standard artificial cerebrospinal fluid (ACSF) at 35°C that was gradually cooled to room temperature. The ACSF solution contained the following (in mM): 126 NaCl, 2.5 KCl, 26 NaHCO3, 2 CaCl2, 2 MgCl2, 1.25 NaH2PO4 and 10 glucose, saturated with carbogen gas. All salts and drugs were obtained from Sigma-Aldrich or Molar Chemicals LTD.

Intracellular recordings

The composition of the intracellular pipette solution was the following (in mM): 110 K-gluconate, 4 NaCl, 20 HEPES, 0.1 EGTA, 10 phosphocreatine, 2 ATP, 0.3 GTP, 3 mg/ml biocytin adjusted to pH 7.3–7.35 using KOH (285–295 mOsm/L). Whole-cell series resistance was in the range of 5–15 MΩ. Series resistance was not compensated but was frequently monitored, and cells where the values changed more than 25% during

recording were discarded from further analysis. Voltage measurements were not corrected for the liquid junction potential. To record GABAergic currents, membrane potential was clamped far (~0 mV) from GABA reversal potential. In case of intracellular recordings, fast glutamatergic transmission was blocked by adding the α-amino-3-hydroxy-5-methyl-4-isoxazolepropionic acid (AMPA)-receptor antagonist NBQX (20 μM; Hello Bio Inc.) and the N-methyl-D-aspartate (NMDA)-receptor antagonist AP-5 (50 μM; Tocris Bioscience) to the recording solution. To test GABAA-receptor dependent synaptic transmission, we administered the GABAA-receptor antagonist gabazine (5 μM; Tocris Bioscience) into the ACSF. All drugs were administered from stock solutions via pipettes into the ACSF containing superfusion system. For ChR2 illumination, we used a blue laser diode (447 nm, Roithner LaserTechnik GmbH) attached to a single optic fiber (Thorlabs) positioned above the hippocampal slice. For ArchT illumination, we used a red laser diode (640 nm, iBeam smart, Toptica Photonics) with optic fiber positioned above NI. Cells recorded in current clamp configuration were depolarized above firing threshold to test the effectivity of ArchT mediated inhibition on action potential generation.

Digital signal processing, analysis and statistics for in vitro experiments

All data were processed and analyzed off-line using self-developed programs written in Python 2.7.0 and Delphi 6.0 by A.I.G. and D.S. In every in vitro experiment, we used median and 25%-75% interquartile range to describe data groups because they did not display a Gaussian distribution.

In vivo two-photon calcium imaging

Calcium imaging in head-fixed, behaving mice was performed using a two-photon microscope equipped with an 8 kHZ resonant scanner (Bruker) and a Ti:Sapphire laser (Chameleon Ultra II, Coherent) tuned to 920 nm. For image acquisition we used a Nikon 40× NIR Apo water-immersion objective (0.8 NA, 3.5 mm WD) coupled to a piezo-electric crystal (Bruker). To adjust the angle of the imaging window to the plane of the front lens of the objective, we set the angle of the fixed-head with two goniometers (Edmond Optics). Fluorescent signals were collected by a GaAsP photomultiplier tube (Hamamatsu 7422P-40) at 1-1.5 × digital zoom covering 300 × 300 μm - 200 × 200 μm with 512 × 512 pixels per imaging plane. To minimize the loss of bouton calcium signals caused by z-motion of the brain, we imaged from 5 planes separated by 2 μm in z at 5 Hz.

Behavior for two-photon calcium imaging

For the in vivo head-fixed 2P calcium-imaging experiments, behavioral training of the mice was started three days after implantation surgery. Mice were hand habituated, water restricted (>90 percent of their pre-deprivation body weight) and trained for 5-7 days to run on a 2 m-long cue-less burlap belt on a treadmill for water rewards, while being head-fixed (gradually decreasing the number of reward zones from 15 covering the full length of the belt to randomly delivered 3 water rewards). Mice were also habituated to the 2P setup and the scanner and shutter sounds prior to the actual 2P imaging experiments. The treadmill was equipped with a lick-port for water delivery and lick detection. Locomotion was recorded by tracking the rotation of the treadmill wheel using

an optical rotary encoder (256 CPR, Bourns). Stimulus presentation and behavioral read-out were driven by microcontroller systems (Arduino), using custom made electronics. During random foraging experiments three water rewards were presented per lap in random locations, while mice were running on a cue-less burlap belt. In salience experiments, discrete stimuli were presented as described (41), with slight modifications. Air-puff (duration: 200 ms, flow rate: 4 LPM), water (duration of valve opening: 200 ms), light (duration: 200 ms, red LED) and tone (duration: 200 ms, frequency: 2500 Hz, from one speaker below the mice) were presented randomly within a 5 s stimulus time, the pre-stimulus time was 5 s, the post-stimulus time was 15 s. Stimuli were repeated 10× for each modality in a pseudorandom order during one experiment.

Two-photon calcium imaging data pre-processing

The acquired 2P imaging data were pre-processed for further analysis using the SIMA software package (76). Motion correction and extraction of dynamic GCaMP6f fluorescent signals were conducted as described (77). Regions of interest (ROIs) were drawn manually over the time-averages of motion corrected time-series to isolate the bouton calcium signals of GCaMP6f-expressing axons. Any imaging frames with residual motion artifacts were excluded from further analysis. Relative fluorescence change (ΔF/F) was calculated by first smoothing the raw fluorescence trace for each ROI with a first-order Savitzky-Golay filter (60 window) to estimate baseline fluorescence. The baseline was then subtracted from the lightly filtered raw fluorescence (1 second window), which was divided by the baseline to obtain ΔF/F.

Analysis of two-photon calcium imaging data

Bouton responses. Peri-event time histograms (PETHs) and peri-stimulus time histograms (PSTHs) were calculated by extracting each bouton's ΔF/F in a window around the onset of each event/stimulus (plotted as -5 to +10 sec around the onset). For the data presented in Fig. 3, we first averaged each ROI's responses across all iterations of the stimulus/event, and then plotted the grand mean of responses across ROIs with a 99% confidence interval via bootstrap resampling. Only boutons with significant responses to the stimulus were included in the plotted PETHs in Fig. 3E or PSTHs in Fig. 3F.

Bouton response significance. We assessed whether a bouton was significantly modulated by each stimulus/event by a bootstrap test. For each presentation of a stimulus or event for a ROI, we calculated the change in fluorescence from five seconds before presentation (Pre) to five seconds after (Post). We then calculated a bootstrapped confidence interval on the average change in fluorescence during stimulus presentation by bootstrap resampling. P-values for each stimulus/ROI pair were calculated as 1 minus the fraction of bootstrapped averages greater than zero (less than zero for the run-stop analysis). ROIs were considered to have a significant response to a stimulus/event if the bootstrapped p-value was < 0.05. This threshold is marked on the summary plots in Fig. 3H-I to denote the proportion of ROIs expected to display significance by chance. We calculated each proportion from the total population of ROIs that responded to at least 1 stimulus, to exclude the fraction of boutons in the FOVs that did not display significant dynamics.

Statistics for two-photon calcium imaging

Statistical differences in bouton fluorescence when mice were stationary and running was tested via Wilcoxon signed-rank test. PSTH significance for each ROI/event pair was determined by a bootstrap test as described. Z-tests were used to compare ROI proportions using the Bonferroni procedure to correct p-values for multiple comparisons, where appropriate.

Jaccard similarity test was carried out on data presented in Fig 3J to assess the significance of the overlap in ROI populations activated by each stimulus pair. Using a permutation test, we tested whether the overlap between the ROIs recruited by each stimulus is any less than what we would expect from random selection of ROIs from the population. We report the p-values from the procedure above for all stimulus pairs.

Optogenetics and contextual fear conditioning (CFC)

After optic fiber implantations, mice were transferred to the animal room of the behavioral unit, where they received 5 days of handling. Behavioral experiments were performed in a separate experimental room. On the 6th day, mice were placed into the first environmental context (environment "A") in a plexiglass shock chamber (25 cm × 25 cm × 40 cm) that was enriched with a specific combination of cues - olfactory (citrus scent), visual (black and white striped wall), spatial (square-shaped chamber), auditory (white noise) and tactile (metal bars on the floor). Mice were allowed to freely move in the first environment for 2 min to record baseline freezing levels. Mice were considered to display freezing behavior, if they did not make any movement other than breathing for at least 2 seconds. After this, mice received 4 foot-shocks (2 seconds, 1-2 mA intensity, 30 seconds inter-shock interval). Optogenetic stimulation (15 mW intensity at the tip of the optic fiber, 5 ms blue laser light pulses at 25 Hz for 6 seconds, at 473 nm wavelength) was precisely aligned with the shocks, starting 2 seconds before shock onset and finishing 2 seconds after shock offset. For the "ChR2-shifted" group, this laser stimulation was shifted by 15 seconds after shock onset. Foot shocks and laser pulses were driven by a custom-made TTL pulse generator (Supertech Instruments). After four successfully delivered shocks, mice were placed back into their home cages for 24 h. On the 7th day, mice were placed back into the first environment for 3 minutes to record freezing behavior. (The shock chamber was cleaned thoroughly with citrus soap between mice). This was followed by 5 days of extensive handling to achieve full fear extinction that reset freezing behavior to a normal baseline. On the 13th day, mice were placed into the second environmental context (environment "B"), composed of another set of cues - olfactory (macadamia nut scent), visual (black dotted walls with white background), spatial (bended chamber walls), auditory (no noise) and tactile (metal bars on the floor) cues. Baseline freezing levels were recorded for 3 minutes, followed by 4 shocks without optogenetic stimulation. After receiving the shocks, mice were placed back into their home cages and the shock chamber was cleaned thoroughly with macadamia nut soap. Then 24 h later, on the 14th day, freezing behavior was recorded in the second environment for 3 minutes. The behavior of the mice was recorded with a JVC GC-PX100 camcorder, and freezing behavior was analyzed manually using the Solomon Coder software. We considered freezing behavior periods as those when mice displayed only respiration-related movements for at least 2 seconds. The experimenter evaluating freezing levels was blinded to the conditions and history of the mice. Mice showing

higher than 5% baseline freezing levels in environment “A” were excluded from further analysis.

Optogenetics and delay cued fear conditioning (CuedFC)

After optic fiber implantations, mice were transferred to the animal room of the behavioral unit of the institute, where they received 5 days of handling. On the 6th day, mice were placed into the first environmental context (environment “A”) in a plexiglass shocking chamber (25 cm × 25 cm × 31 cm) that was enriched with a specific combination of cues - olfactory (macadamia nut scent), visual (black dotted wall with white background), spatial (bended chamber walls), auditory (white noise) and tactile (metal bars on the floor). Mice were allowed to freely move in the first environment for 3 minutes to record baseline freezing levels. After this, mice received 3 shocks (2 seconds, 2 mA intensity, 60 seconds inter-shock interval) that were paired with an auditory cue (30s long sound at 7500 kHz). The footshocks and the auditory cues were co-terminated each time. After receiving the last shock, mice were kept in the context for another 30 seconds. During the experiment, lasting 6 minutes, mice received a continuous yellow laser light illumination (15 mW intensity at the tip of the optic fiber at 593 nm wavelength). After 3 successfully delivered shocks, mice were placed back into their home cages for 24 h. On the 7th day, mice were placed back into the first environment for 3 minutes to record freezing behavior related to the contextual fear memories. Then 24 h later, on the 8th day, mice were placed into a second environmental context (environment “B”) with distinct cues - olfactory (citrus scent), visual (black and white striped wall), spatial (square shaped chamber), auditory (no noise) and tactile (plastic floor). Here, after 3 minutes mice were presented with the auditory cue for 1 minute to record freezing behavior related to the cued fear memories. The behavior of mice was recorded with a JVC GC-PX100 camcorder, and freezing behavior was analyzed manually using the Solomon Coder software. The experimenter evaluating freezing levels was blind to the conditions of the mice. Mice displaying higher than 5% baseline freezing levels in environment “A” were excluded from the further analysis.

Elevated plus maze (EPM) after optogenetic CFC

One (1) hour after freezing behavior assessment in the first environment (7th day) we placed the mice into an EPM to test their anxiety levels. The cross-shaped EPM apparatus consisted of two open arms with no walls (30 cm × 7 cm) and two closed arms (30 cm high walls) and was on a pedestal 50 cm above floor level (Fig. 6A). The behavior of the mice was recorded with a JVC GC-PX100 camcorder and evaluated using an automated system (Noldus Ethovision 10.0; Noldus Interactive Technologies). Behavior was measured as total time in the open and closed arms.

Statistics for optogenetic behavioral experiments

In every behavioral experiment, we used median and 25%-75% interquartile range to describe data groups, because they did not display a Gaussian distribution. To test for statistically significant differences in independent data populations, we used the Mann-Whitney U-test, and in dependent data populations, we used the two-sided Wilcoxon signed-rank test.

In vivo electrophysiological recordings in freely behaving mice

Electrophysiological recordings were commenced after a 7-day post-surgery recovery and habituation to 'connectorization'. The signal from the silicon probe was multiplexed by RHA2132 chip (Intan Technologies, Los Angeles, CA, USA) and transmitted through a lightweight flexible cable to the signal acquisition system (KJE-1001, Amplipex Ltd, Szeged, Hungary) at 20 kHz sampling rate. The movement of the mouse was tracked by a marker-based, high speed (120 frame/s) 4-camera motion capture system and reconstructed in 3D (Motive, OptiTrack, NaturalPoint Inc, Corvallis, OR, USA). The markers needed for tracking were attached to the headstage connected to the silicon probe and to the shielding mesh. After home cage recording, mice were placed into an open arena (40 × 60 cm) and into a linear track (100 × 9 cm). Recordings were repeated 1-7 days later. In each recording situation, blue (473 nm) light stimulation was triggered manually by the experimenter controlling the TTL pulse generator (Spike2 and micro1401mkII, CED Ltd, Cambridge, UK). Various trains of 5 ms long TTL pulses were used: constantly repeating at 5, 15 or 25 Hz frequency (50-100 pulses in total per session) or delivered in a theta burst protocol (TBS, 3 or 5 pulses at 25 or 50 Hz in bursts repeated at 5 or 10 Hz). TTL pulses were fed into the power supply of the laser (IKE-473-LN-100T with a power supply (IKE-PS-300, IkeCool Corp, Anaheim, CA, USA) coupled to a 105 μm core diameter multi-mode patch cable (Thorlabs GmbH, Dachau/Munich, Germany) terminating in a ceramic ferrule. This ferrule was connected by a ceramic mating sleeve to either the incertus-implanted or the control optical fiber, plus the mating sleeve was covered by a small black plastic tube to minimize the light leakage. The light intensity at the tip of the fiber was approximately 9-13 mW prior to recordings. Mice were recorded in 3 - 9 sessions for 2 - 5 weeks. Mice were perfused transcardially with 4%PFA after the electrophysiological recordings were completed, and the brains were processed for histological verification of the viral transduction zone and implantation. Data from mice with confirmed transduction, optical fiber position and silicon probe track colored by DiI (Molecular Probes, Cat. No.: D282) prior to the implantation were used in the analysis (n = 5).

Data analysis and statistics for in vivo experiments

The analysis was performed in MATLAB environment (MathWorks, Natick, MA, USA) by custom-written functions and scripts. Local field potential (LFP) signal was downsampled at 1 kHz. Channels from strata pyramidale, radiatum, lacunosum-moleculare, moleculare and hilus were identified by characteristic physiological markers (amplitude of ripple activity, reversal of sharp-waves, phase-shift of theta oscillation and sink-source distribution on current source density profiles) and probe track location in histological preparations. The instant speed of the mouse was calculated from the 3D-tracked position data synchronized to the LFP recordings. To reduce the velocity noise, the harmonic mean of instant speed (calculated by overlapping 11-sample sliding segments, omitting speed data when the increment of instant acceleration was more than 5-fold) smoothed by a Savitzky-Golay filter (occasional negative values in the result were replaced by the linear interpolation between surrounding positive values) was used in the analysis. The stimulation sessions were categorized by whether the mouse was running or sleeping in REM state at the illumination onset. The criteria for running episodes were: (a) average speed of the mouse in 4 subsequent 0.5 s long time segments preceding the

stimulus onset above 4 cm/s and (b) higher power in theta band (5-12 Hz) than in delta band (1-4 Hz) assessed by the Welch's power spectral density estimate (periodogram) of the pyramidal LFP in the 2 s preceding the stimulus onset. The criteria for REM sleep episodes were: (a) absence of synchronous activity in the 300-1000 Hz band of LFP across all neighboring channel pairs, (b) average speed below 4 cm/s and (c) higher power in theta band than in delta band of LFP (the last two criteria were measured by the same method as detailed above in the running definition). Running episodes were pooled together from recordings made in the open arena and linear track, REM episodes were identified in home cage recordings. LFP changes in the pyramidal layer of CA1 induced by the optical stimulations were assessed by the ratio of spectral power distribution calculated by Welch's overlapped segment averaging estimator during the illumination and the preceding 2 s. Changes in low (5-8 Hz) and high theta (8 - 12 Hz) band activity (spectral power was summed in the given frequency range) among different stimulation protocols were compared by one-way Kruskal-Wallis ANOVA followed by Tukey's honestly significant difference procedure. The effects of the stimulation protocol that evoked significantly stronger power change in the high theta band than other in protocols (i.e., 25 Hz stimulation conducted in n = 4 mice, both NI GABAergic neuron and control illumination) were detailed in further analysis steps. In addition to low and high theta band, spectral power changes of the pyramidal LFP in the range of slow gamma (here restricted to 30-45 Hz to exclude rhythms generated by the repeating light-pulse-evoked transients at 25 Hz and its harmonics such as 50 Hz) and mid gamma (60-100 Hz) were also examined. Time-frequency decomposition of pyramidal LFP with continuous wavelet transform (78) and subsequent bias correction of spectral power (79) was used to calculate instant power. Pairing of instant power and speed data during stimulation, and the preceding and following 4 s allowed us to disparately examine the changes in the low and high theta band power when mice were quiet (instant speed: 0-4 cm/s) and moving (instant speed > 4 cm/s). Current source density (CSD) maps were calculated to uncover electric responses upon stimulation in more superficial layers of CA1 such as stratum radiatum and lacunosum-moleculare and in the dentate gyrus. For CSD analysis, noisy and low impedance channels were excluded manually. Pulse-onset-triggered CSD averages were calculated in ±100 ms around the onset of light pulses during stimulation, and for the preceding 2 s, the intervals of the original pulse train were shifted with a random start time. Theta-peak-triggered CSD averages were calculated in ±250 ms around the peaks of theta cycles (the phase was computed from the Hilbert transform of 8 - 12 Hz band filtered pyramidal LFP signal) when instant power of pyramidal theta oscillation was higher than that of delta (the power ratio was computed from bias-corrected time-frequency decomposition of LFP with continuous wavelet transform). For assessment of stimulation-induced current changes, data were temporally (in ±10 ms around the maximal sink following the onset of pulses or the peaks of theta cycles) and spatially (channels in the same layer of hippocampus) averaged. For visualization purposes only, CSD maps were smoothed by a Gaussian filter after 100-times linear interpolation between each channels. For statistical comparisons of in vivo physiological data, non-parametric two-sided Wilcoxon rank sum (control vs. NI GABAergic neuron stimulation) and signed-rank tests (before vs. during stimulation or during vs. after stimulation) were used.

Data and code availability

Data generated and analysed during the current study are presented in the manuscript or in the Supplementary Materials file, while additional datasets and custom written codes for in vivo electrophysiological recordings, 2P-imaging and data analysis are available from the following links: https://figshare.com/s/9fb345fc23ac2ac94fcd and https://figshare.com/s/5b0c6be2431caf10272b

Supplementary Text for Main Figures 1-6

Supplementary Data for Main Fig. 1

Figure 1C: The vast majority of eYFP-positive fibers was positive for relaxin-3 (at least 194/210) and vGAT (at least 351/357, white arrowheads), and the majority of the relaxin-3 positive boutons also contained eYFP- (at least 388/410) and vGAT-positivity (at least 402/410), indicating that effectively all relaxin-3-containing fibers targeting the hippocampus originate from the NI.

Figure 1D: Synapses established by the NI were positive for the GABAA-receptor γ2 subunit (at least 35/48, upper row) and the scaffolding protein gephyrin (at least 55/62, lower row). The sizes of synapses established by NI neurons were measured on the immunoreactions for gephyrin, on fully reconstructed synapses from 70 nm thick serial sections. Synapse areas are given (in µm2) as follows (median [25%-75% quartiles]): CA1 (n=19): 0.22 [0.12-0.39]; hilus (n=17): 0.22 [0.19-0.25].

Figure 1I: The majority of relaxin-3 positive NI fibers establish synaptic contacts marked by gephyrin on SOM-positive interneurons in the hippocampus (at least 264/424).

Figure 1J: The in vitro recorded neurons in the stratum oriens (n=18) were post-hoc characterized morphologically (6 O-LM cells [4 of them confirmed SOM positive], 4 projection cells, 1 bistratified cell, 7 unidentified cells) and neurochemically (at least 12/18 SOM-positive cells).

Figure 1N: IPSC amplitudes (in pA) are as follows (median [25%-75% quartiles]): control (red): 32.74 [30.75-44.59], gabazine (blue): 0 [0-0], washout (yellow): 18.45 [11.91-25.25].

Supplementary Data for Main Fig. 2

Figure 2C: The majority of eYFP-positive fibers was positive for relaxin-3 (at least 154/241) and vGAT (at least 212/241), and the majority of the relaxin-3 positive boutons also contained eYFP- (at least 169/190) and vGAT-immunoreactivity (at least 187/190), indicating that effectively all relaxin-3-containing fibers targeting the hippocampus arise from the NI.

Figure 2D: NI synapses in the MS, contained the GABAA-receptor γ2 subunit (at least 28/28, upper row) or the scaffolding protein gephyrin (at least 43/44, lower row. The sizes of synapses established by NI were measured on the basis of immunoreactions for gephyrin, on fully reconstructed synapses from 70 nm serial sections. Synapse areas are given (in µm2) as follows (median [25%-75% quartiles]): MS (n=32): 0.24 [0.19-0.29].

Figure 2F: At least 148/270 relaxin-3 positive terminals established synapses with vGluT2-positive profiles. The majority of medial septal vGluT2-positive cells received at least one such contact in the examined area (at least 45/80 counted cells).

Figure 2H: At least 21/280 relaxin-3 positive terminals contacted ChAT-positive cell profiles. Medial septal ChAT-positive neurons received at least one such contact in the examined area (at least 14/38 counted cells).

Supplementary Data for Main Fig. 4

Figure 4C: Abbreviations: A24a: cingulate cortex area 24a; A24b: cingulate cortex area 24b; ATg: anterior tegmental nucleus (Gudden); DMTg; dorsomedial tegmental nucleus; DR: dorsal raphe; DTg: dorsal tegmental nucleus; Gi: gigantocellular nucleus; HDB: horizontal limb of the diagonal band of Broca; iRt: isthmic reticular formation; LDTg: laterodorsal tegmental nucleus; LH: lateral hypothalamus; LHb: lateral habenula; LPo: lateral preoptic area; MM: mammillary bodies; MRR: median raphe region; mRt: mesencephalic reticular formation; MS:medial septum; NPr: nucleus prepositus; PAG: periaqueductal grey matter; PH: posterior hypothalamus; PNO: nucleus pontis oralis; SIB: substantia innominata of the basal forebrain; SUM: supramammillary nucleus; VDB: vertical limb of the diagonal band of Broca; VTA: ventral tegmental area; ZI: zona incerta

Supplementary Data for Main Fig. 6

Figure 6A: Population data for the freezing levels (in % of total time) in the environment ”A” for n=9 ChR2 and n=10 CTRL mice that received foot-shock-aligned stimulation of NI are as follows: (median [25%-75% quartiles]): ChR2: 1.22 [0.00-2.45], CTRL: 13.63 [5.01-21.36] (**: p=0.003, Mann-Whitney U-test).

Population data for the time spent in open arms of the EPM (in seconds) for n=7 ChR2 and n=10 CTRL mice that received foot-shock-aligned stimulation of NI are as follows: (median [25%-75% quartiles]): ChR2: 34.36 [18.64-97.44], CTRL: 12.00 [0.88-23.76] (*: p=0.022, Mann-Whitney U-test).

Figure 6B: Population data for the freezing levels (in % of total time) for n=21 ChR2 mice that received foot-shock-aligned stimulation of NI fibers in the HIPP, are as follows: (median [25%-75% quartiles]): environment ”A”: 3.67 [2.22-6.34], environment ”B”: 12.01 [4.78-18.24] (**: p=0.007, Wilcoxon signed-rank test).

Population data for the freezing levels (in % of total time) for n=14 CTRL mice that received foot-shock-aligned stimulation of NI fibers in the HIPP are as follows: (median [25%-75% quartiles]): environment ”A”: 6.67 [0.00-19.02], environment ”B”: 15.63 [5.90-18.13] (n.s.: non-significant, p=0.196, Wilcoxon signed-rank test).

Figure 6C: Population data for the freezing levels (in % of total time) for n=6 ChR2-light-aligned and n=6 ChR2-light-shifted mice, are as follows: (median [25%-75% quartiles]): ChR2-aligned: 4.34 [2.22-6.56], ChR2-shifted: 20.86 [8.79-25.36] (**: p=0.008, Mann-Whitney U-test).

Figure 6D: Population data for the contextual freezing levels (in % of total time) in the environment ”A” for n=5 ArchT and n=6 CTRL mice are as follows: (median [25%-75% quartiles]): ArchT: 15.11 [13.67-17.56], CTRL: 6.11 [4.11-8.67] (*: p=0.022, Mann-Whitney U-test).

Population data for the cued freezing levels (in % of total time) in the environment ”B” for n=5 ArchT and n=6 CTRL mice are as follows: (median [25%-75% quartiles]): ArchT: 36.50 [33.33-39.67], CTRL: 40.33 [32.00-52.67] (n.s.: non-significant, p=0.784, Mann-Whitney U-test).

Fig. S1. Supplementary anatomical details of NI GABAergic neuronal projections

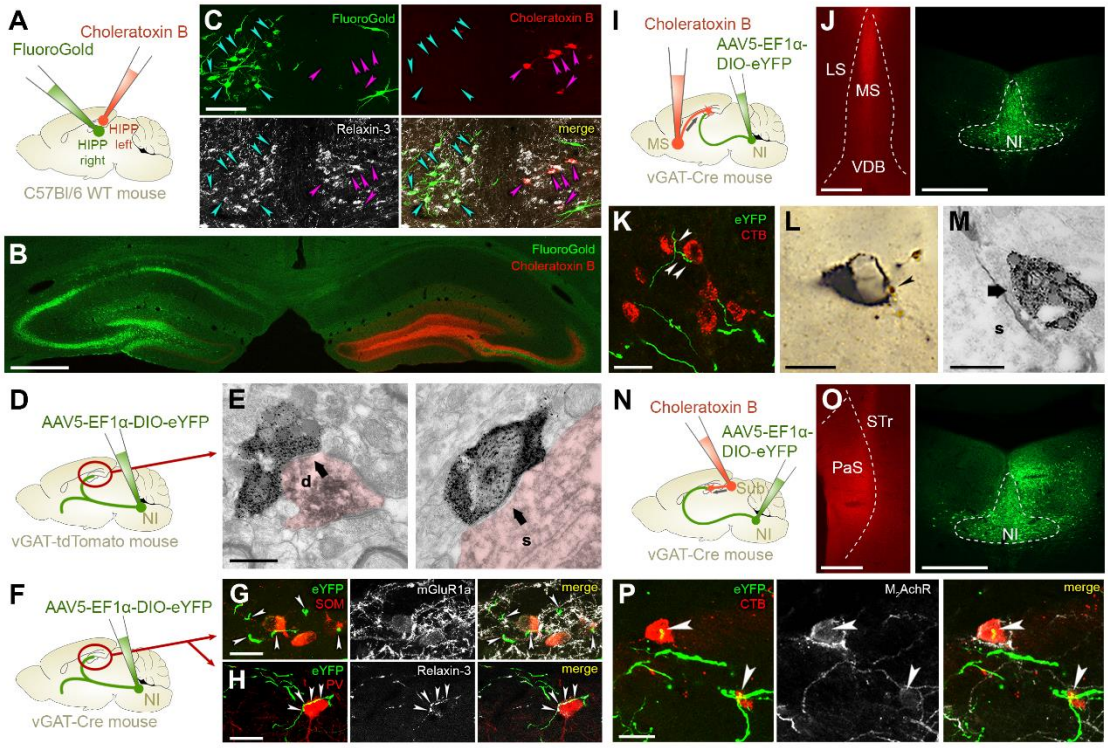

A: Double retrograde tracing in the bilateral hippocampi using FG in the right and CTB in the left hemisphere, respectively, in C57Bl/6 wild-type mice (n=2).
B: A representative injection site illustrating green FG labeling and red CTB labeling in the hippocampi of right and left hemispheres, respectively. Scale bar: 500 µm.
C: FG labeled neurons (green, cyan arrowheads) and CTB labeled neurons (red, magenta arrowheads) are mainly located in the ipsilateral NI, in the right or left hemisphere, respectively. Only a few NI neuron were positive for both retrograde tracers (18/315). The majority of the retrogradely-labeled neurons was relaxin-3 positive (white, 222/315). Scale bar: 100 µm.
D: AAV2/5-EF1α-DIO-eYFP was injected into the NI of vGAT-tdTomato reporter mice (n=2).
E: Electron microscopic images reveal SI-DAB (grainy precipitate) containing NI fibers establishing symmetrical synaptic contacts (black arrows) with DAB-Ni (dark precipitate, false-colored with faint red) containing hippocampal interneuron dendrites (d) and somata (s). The majority of NI fibers established synaptic contacts with DAB-Ni positive GABAergic profiles (total: 62/71, 55 on dendrites, 7 on somata). Scale bar: 600 nm.
F: AAV2/5-EF1α-DIO-eYFP was injected into the NI of vGAT-Cre mice (n=7).
G: NI fibers labeled with eYFP (green) establish putative contacts (white arrowheads) with SOM-positive (red) and mGluR1α-positive (white) interneurons in the stratum oriens of the dorsal CA1. Scale bar: 20 µm.
H: Many of the SOM-positive interneurons are parvalbumin (PV)-positive in stratum oriens of HIPP. NI fibers labeled with eYFP (green) and positive for relaxin-3 (white)

establish putative contacts (white arrowheads) with a PV-positive interneuron (red) in the stratum oriens of the dorsal CA1. Scale bar: 20 μm.
I: AAV2/5-EF1α-DIO-eYFP was injected into the NI and CTB was injected into the MS of the same vGAT-Cre mice (n=2) to label hippocamposeptal projection neurons.
J: Representative injection sites illustrating red CTB labeling in the MS and green eYFP labeling in the NI. Abbreviations: LS: lateral septum; MS: medial septum; VDB: ventral limb of the diagonal bands of Broca. Scale bars: 500 μm.
K: eYFP-positive NI fibers in the HIPP (green) establish putative contacts (white arrowheads) with CTB-positive hippocamposeptal interneurons (red). Scale bar: 20 μm.
L: A NI fiber labeled with brown SI-DAB establishes a synaptic contact with a CTB-positive hippocamposeptal interneuron labeled with black DAB-Ni precipitate in the DG. The NI terminal reconstructed with correlated light- and electron microscopy is indicated with a black arrowhead. Scale bar: 10 μm.
M: The same terminal marked in S also has a symmetrical synaptic contact (black arrow) on the soma (s) of a hippocamposeptal interneuron. Scale bar: 600 nm.
N: AAV2/5-EF1α-DIO-eYFP was injected into the NI and CTB was injected into the subiculum of the same vGAT-Cre mice (n=2) to label hippocampo-retrohippocampal projection neurons.
O: Representative injection sites illustrating red CTB labeling in the subiculum and green eYFP labeling in the NI. Abbreviations: PaS: parasubiculum; STr: subiculum, transition area. Scale bars: 500 μm.
P: eYFP-positive NI GABAergic fibers in the HIPP (green) establish putative contacts (white arrowheads) with CTB-positive hippocampo-retrohippocampal interneurons (red), which are also positive for the type 2 muscarinic acetylcholine receptor (M2AChR, white). Scale bar: 20 μm.

Fig. S2 Projection patterns of NI and surrounding nuclei

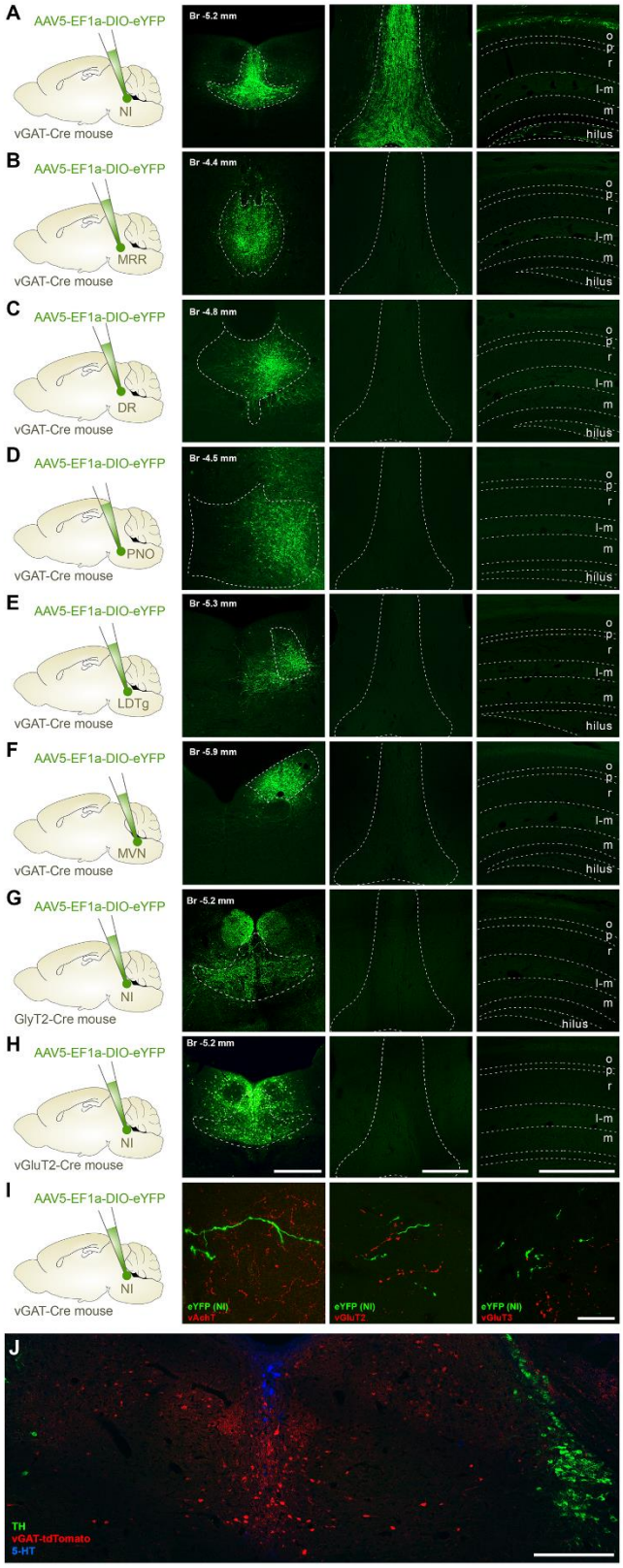

A-H: AAV2/5-EF1α-DIO-eYFP was injected into various areas in the brainstem in vGAT-Cre, vGluT2-Cre or GlyT2-Cre mice. The images illustrate representative coronal sections from the region of the different injection sites and from the hippocampus and MS, respectively. The centers of the injection sites were also identified and defined by their anteroposterior coordinates from Bregma. Note, that the characteristic vGAT-positive fiber labeling of the NI in these forebrain areas can be observed only in vGAT-Cre mice (A), and it is absent, when the AAV-eYFP was injected into the neighboring brain areas or into vGluT2-Cre or GlyT2-Cre mice. Scale bars (panel H) 500 μm for all images (columns of A-H).
A: AAV2/5-EF1α-DIO-eYFP was injected into the nucleus incertus (NI) of vGAT-Cre mice (n=7).
B: AAV2/5-EF1α-DIO-eYFP was injected into the median raphe region (MRR) of vGAT-Cre mice (n=2).
C: AAV2/5-EF1α-DIO-eYFP was injected into the dorsal raphe (DR) of vGAT-Cre mice (n=2).
D: AAV2/5-EF1α-DIO-eYFP was injected into the nucleus pontis oralis (PNO) of vGAT-Cre mice (n=2).
E: AAV2/5-EF1α-DIO-eYFP was injected into the laterodorsal tegmental nucleus (LDTg) of vGAT-Cre mice (n=2).

F: AAV2/5-EF1α-DIO-eYFP was injected into the medial vestibular nucleus (MVN) of vGAT-Cre mice (n=2).
G: AAV2/5-EF1α-DIO-eYFP was injected into the NI of GlyT2-Cre mice (n=2).
H: AAV2/5-EF1α-DIO-eYFP was injected into the NI of vGluT2-Cre mice (n=2).
I: AAV2/5-EF1α-DIO-eYFP was injected into the nucleus incertus (NI) of vGAT-Cre mice (n=2). We did not observe any meaningful co-localization of AAV-eYFP containing NI fibers and vesicular acetylcholine transporter (vAChT, only 3/320) or vGluT2 (only 3/206) or vGluT3 (0/216) in the dorsal CA1 of the hippocampus, measured in n=2 mice per reaction, respectively. The apparent labeling was likely false positives. Scale bar: 20 μm for all images per row.
J: A representative coronal section from the pons of a vGAT-tdTomato mouse (n=2 mice tested) illustrates that GABAergic neurons of the NI (red) do not co-express tyrosine-hydroxylase (TH, green) or serotonin (5-HT, blue). Scale bar: 250 μm.

Fig. S3 Supplementary data from in vitro recordings of NI GABAergic cells

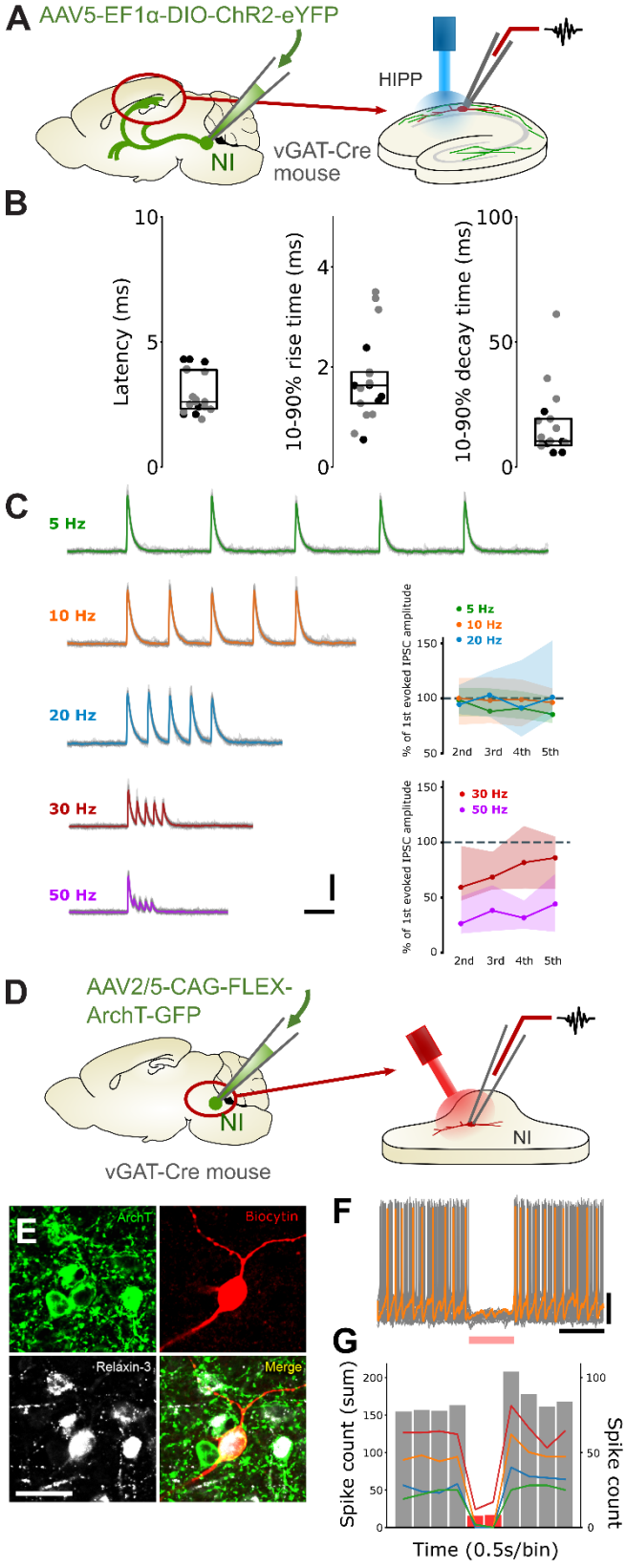

A: Experimental design of optogenetic in vitro intracellular recordings (experiment described in detail in Fig. 1J).
B: Population data (n=18 cells) for in vitro recorded IPSC latencies (defined as time between stimulus onset and 10% of IPSC amplitude), 10-90% rise times and 10-90% decay times. Data are presented (in ms) as follows (median [25%-75% quartiles]): Latency: 2.6 [2.3-3.55], 10-90% rise time: 1.63 [1.28-1.89], 10-90% decay-time: 11.11 [8.77-19.02]. Black dots represent cells that could be both reconstructed and identified as OLM cells.
C: Left panel displays averaged IPSCs from the O-LM cell in Fig. 1K. Optical stimulation was delivered at 5 Hz (green), 10 Hz (yellow), 20 Hz (blue), 30 Hz (red) and 50 Hz (purple) to test frequency-dependent short-term plasticity. At lower (5-20 Hz) frequencies, no short-term plasticity was evident. The cell displayed STD at higher (30-50 Hz) stimulation frequencies, although it is not clear whether ChR2 stimulation-failure at these higher 50 Hz frequencies may have contributed to an increased STD. Scale bars: 100 ms, 200 pA.
Right panel: population data showing changes in amplitudes for 17 cells are as follows (median [25%-75% quartiles]): 5 Hz: 2nd 98.65 [83.66-109.43], 3rd 88.22 [83.95-109.43], 4th 91.17 [81.57-106.88], 5th 85.54 [77.57-101.30]; 10 Hz: 2nd 99.87[76.23-118.95], 3rd 98.25 [77.38-119.10], 4th 99.14 [74.52-117.21], 5th 96.28 [89.98-109.05];

20 Hz: 2nd 94.33 [85.83-112.23], 3rd 103.25 [83.24-124.86], 4th 91.29 [65.20-135.02], 5th 100.83 [83.11-152.76], 30 Hz: 2nd 59.40 [46.94-96.68], 3rd 68.44 [57.20-91.52], 4th 81.72 [58.09-114.66], 5th 85.98 [57.73-105.00] and 50 Hz: 2nd 26.48 [17.24-51.00], 3rd 38.37 [19.77-60.98], 4th 31.68 [21.82-47.16], 5th 44.27 [18.81-71.62].
D: Experimental design of optogenetic in vitro intracellular recordings from NI cells. AAV2/5-CAG-FLEX-ArchT-GFP was injected into the NI of a vGAT-Cre mouse (n=1). After 6 weeks of survival, 300-µm-thick horizontal slices containing NI were cut from the brainstem and transferred into a dual-superfusion chamber. NI neurons were whole-cell patch clamped in current clamp mode, and the firing activity of the neurons was measured, while the slices were illuminated with red light. The recorded neurons (n=4) were post-hoc characterized neurochemically (3 were confirmed to be relaxin-3 positive).
E: Confocal laser scanning fluorescent image illustrates a representative GABAergic NI neuron expressing ArchT (green) that was recorded and filled with Biocytin (red). The neuron was positive for relaxin-3. Scale bar: 20 µm.
F: In vitro red-light illumination effectively blocked action potential generation in the GABAergic NI neuron shown in D. Twenty (20) overlaid membrane potential traces are shown with 1 sec-long illumination periods (orange bar). A sample trace is provided (yellow). Scale bars: 1s, 20 mV.
G: Population data illustrating action potential blockade upon illumination of NI neurons expressing ArchT (80 stimulation periods from 4 cells). Cumulative spike count is represented by bars, while individual cell spike counts are represented by lines. Yellow line indicates the cell shown in D-E.

Fig. S4 Injection sites and optic fiber localizations

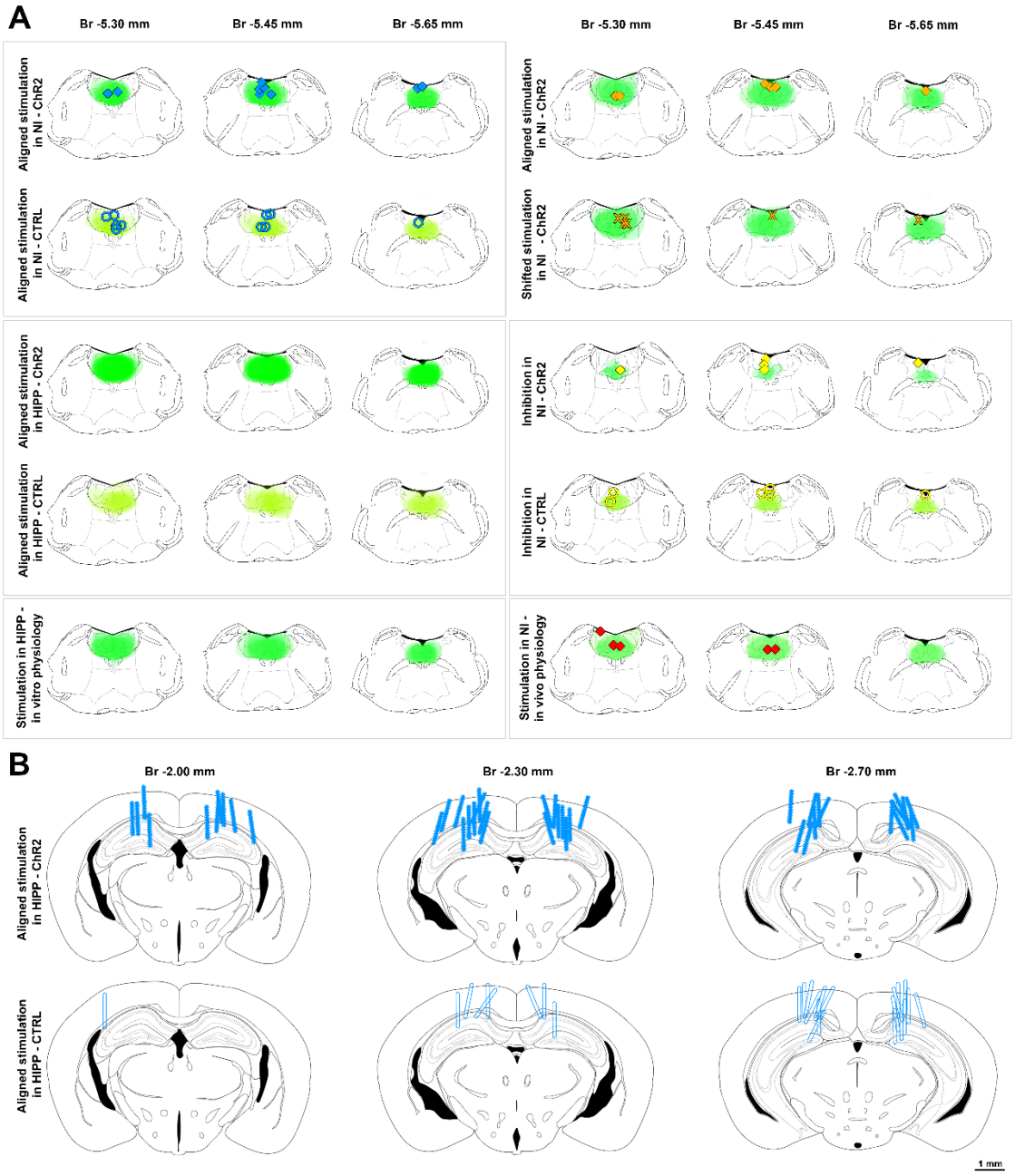

A: Summary of virus injection sites in every mouse used in the behavioral, in vivo or in vitro optogenetic experiments. The virus injection sites in the different mice participating in the different experiments were checked one-by-one and overlaid onto each other. AAV2/5-EF1a-DIO-ChR2-eYFP (ChR2) or AAV2/5-CAG-FLEX-ArchT-GFP (ArchT) expression is labeled with green, AAV2/5-EF1a-DIO-eYFP (CTRL) expression is labeled with yellow in the area of NI and adjacent structures at 3 different coronal levels (Bregma -5.30, -5.45 and -5.65 mm, respectively). The tips of the optic fibers positioned over the NI are also labeled as follows:

- Experiments comparing foot-shock-aligned ChR2 vs. CTRL stimulation in the NI (described in Fig. 6A):
Blue rhombs: optic fibers in ChR2-expressing mice, foot-shock-aligned stimulation.
Blue circles: optic fibers in CTRL-expressing mice, foot-shock-aligned stimulation.
- Experiments comparing foot-shock-aligned stimulation vs. 15 seconds-shifted stimulations in the NI (described in Fig. 6C):
Orange rhombs: optic fibers in ChR2-expressing mice, foot-shock-aligned stimulation.
Orange "X"-s: optic fibers in ChR2-expressing mice, foot-shock-shifted stimulation.
- Experiments comparing ArchT vs. CTRL inhibition (described in Fig. 6D):
Yellow rhombs: optic fibers in ArchT-expressing mice, inhibition.
Yellow circles: optic fibers in CTRL-expressing mice, inhibition.
- In vivo physiology experiments (described in Fig. 6 and Fig. S4):
Red rhombs: optic fibers in ChR2-expressing mice, stimulation in the in vivo physiology experiments.
B: Positions of the etched optic fibers at 3 different coronal levels (Bregma -2.00, -2.30 and -2.70, respectively) in experiments comparing foot-shock-aligned ChR2 vs. CTRL stimulation in the HIPP (described in Fig. 6B):
Blue multiple-pointed filled rods: etched optic fibers in ChR2-expressing mice, footshock-aligned stimulation.
Blue empty rods: etched optic fibers in CTRL-expressing mice, foot-shock-aligned stimulation.

Fig. S5 In vivo hippocampal recordings during optogenetic stimulation of NI GABAergic cells

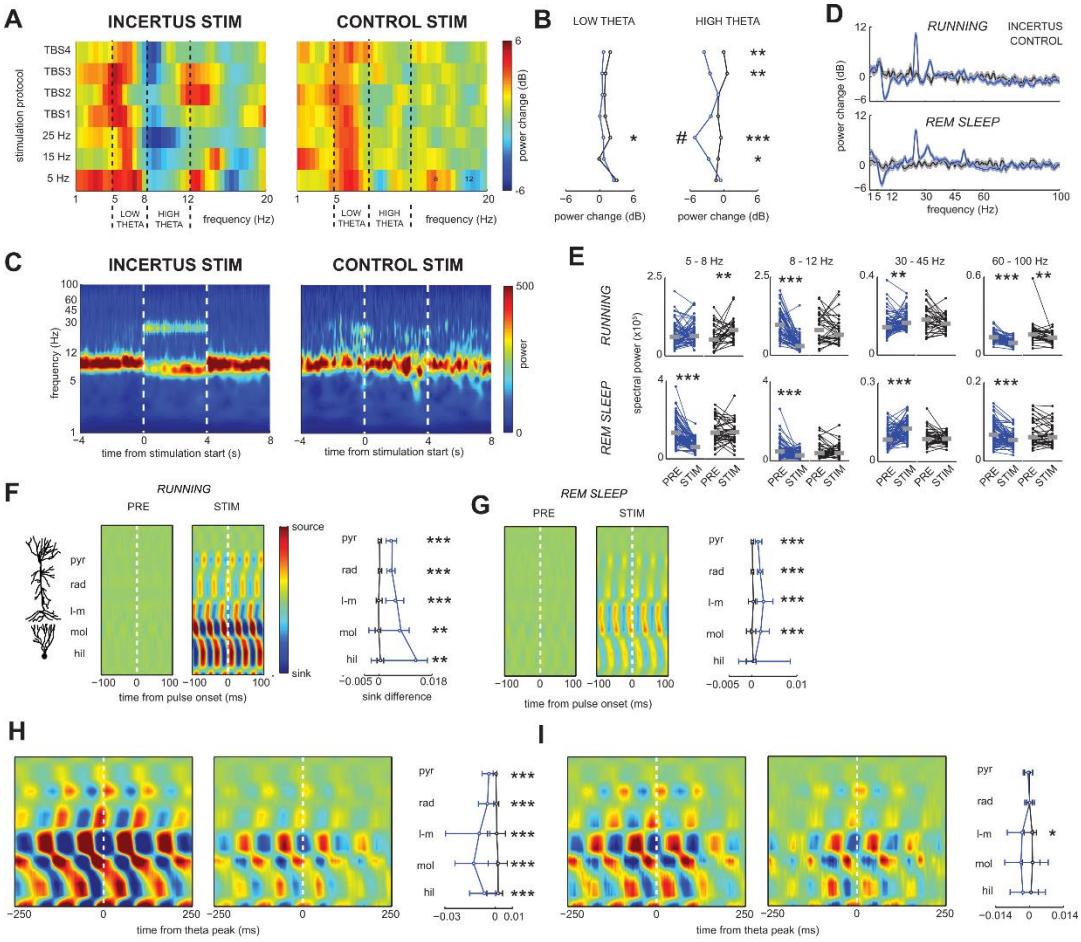

A: Average spectral power change determined as the ratio of Welch's periodograms (spectral power distribution calculated by Welch's overlapped segment averaging estimator) of pyramidal LFP to the preceding 2 seconds-long non-stimulated segment during various stimulation protocols. Running episodes were selected during NI GABAergic neuron (INCERTUS, left) and control stimulations (CONTROL, right). TBS: theta burst stimulation, TBS1: 3 pulses at 25 Hz in bursts repeated by 5 Hz, TBS2: 3 pulses at 50 Hz in bursts repeated by 5 Hz, TBS3: 5 pulses at 50 Hz in bursts repeated by 5 Hz, TBS4: 3 pulses at 50 Hz in bursts repeated by 10 Hz.
B. Changes of summed spectral power in low theta (5-8 Hz, left) and high theta (8-12 Hz, right) bands. Plots show medians of data in rows corresponding to stimulation protocols in A (blue: NI GABAergic neuron stimulation, black: control stimulation). Significant effect of various stimulation protocols on high theta band power was revealed by Kruskal-Wallis ANOVA ($\chi 2(6) = 40.9278$, $p < 0.001$ for NI GABAergic neuron stimulation and $\chi 2(6) = 3.229$, $p = 0.7796$ for control stimulation). Post-hoc test (Tukey's honestly significant difference procedure) proved that 25 Hz stimulation (marked by #) had a significantly different effect to the other protocols. In contrast, these stimulation

protocols had no statistically different effect on low theta band power (Kruskal-Wallis ANOVA, $\chi 2(6) = 3.7744$, $p = 0.7072$ for NI GABAergic neuron stimulation and $\chi 2(6) = 4.0376$, $p = 0.6716$ for control stimulation). On the right side of the plots, significant differences between NI GABAergic neuron and control stimulations are indicated (*: $p < 0.05$, **: $p < 0.01$, ***: $p < 0.001$ two-sided Wilcoxon rank sum test).
C. Time-resolved spectral changes during 25 Hz stimulation demonstrated by the continuous wavelet transform of the pyramidal layer LFP. Here, the same data are illustrated as in Fig. 6B, but the frequency scale is expanded to 100 Hz. Notably, besides theta suppression, the power of the 25-30 Hz band was increased by NI GABAergic neuron stimulation. However, this effect might have resulted from the interaction of incertus-triggered oscillations and rhythms accompanying the stimulation-induced brain state change (e.g. slow gamma).
D. Ratio of Welch's periodograms of pyramidal layer LFP during 25 Hz NI GABAergic cell (blue) and control stimulation (black) to the preceding 2 seconds-long non-stimulated segment (expressed in dB). Mean ± SEM for all stimulations when mice ($n = 4$) were running (top) or sleeping in REM state (bottom) are shown. Reduction in theta power can be detected by wavelet-based decomposition. Additional two peaks of increased activity at 25 and around 30 Hz can also be distinguished, the latter might reflect elevated slow gamma activity.
E. Pyramidal spectral band power (frequency range indicated above the graphs) computed by Welch's method during 25 Hz stimulation (STIM) and preceding 2 seconds-long non-stimulated segment (PRE). Data of all individual stimulation sessions when mice were running (top) or sleeping in REM state (bottom) are plotted (blue: NI GABAergic neuron stimulation, black: control stimulation). Grey lines indicate group medians, significant differences between data groups are indicated (**: $p < 0.01$, ***: $p < 0.001$, two-sided Wilcoxon signed-rank test). Suppression of higher theta band (8-12 Hz) activity, also shown in Fig. 6C by wavelet-based decomposition, is confirmed, and additionally, oscillation around 30 Hz distinct from the evoked activity at 25 Hz was significantly stronger during stimulation than in preceding period (power in 30 - 45 Hz band).
F-I. Depth profile of hippocampal electrical activity. On the left side of every image, current source density maps of averaged LFP from a mouse during NI GABAergic neuron stimulation (STIM) and preceding 2 seconds-long non-stimulated segment (PRE) are shown. Schematic principal neurons of CA1 and dentate gyrus were arranged to the corresponding recording sites of the silicon probe. On the right side of every image, averaged difference of maximal sinks (STIM-PRE) during all 25 Hz NI GABAergic neuron (blue) and control (black) stimulations in $n = 4$ mice are displayed as group medians and 25th - 75th percentile range. Significant difference between NI GABAergic neuron and control stimulations are indicated (*: $p < 0.05$, **: $p < 0.01$, ***: $p < 0.001$, two-sided Wilcoxon rank sum test). Current source density maps are averaged by the individual stimulation pulses repeated at 25 Hz (F, G), or by the peaks of pyramidal layer theta cycles (H, I) in running (F, H) or REM sleep episodes (G, I). White dashed lines on the maps indicate the pulse onset (F,G), or the peak of the theta cycle (H,I).
Abbreviations: pyr: stratum pyramidale; rad: stratum radiatum; l-m: stratum lacunosum-moleculare; mol: stratum moleculare; hil: hilus.

Fig. S6 Supplementary control data for contextual fear conditioning experiments

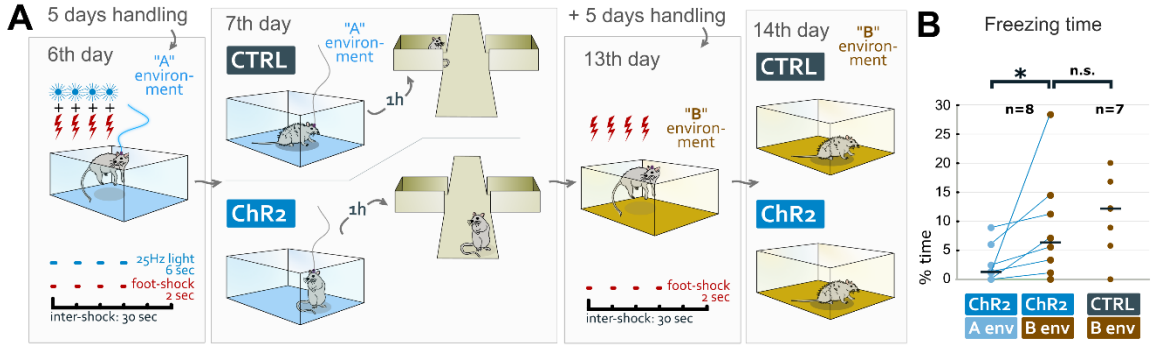

A: Illustration of the experimental design that was used as an additional control for experiments described in Fig. 6A. ChR2- or CTRL-mice were placed into a multisensory context (environment ”A”) to receive foot-shocks and foot-shock-aligned optogenetic stimulation of NI. On the 6th day, freezing behavior in environment ”A” was analyzed, followed by assessment of anxiety levels in the elevated plus maze, 1 hour later. After 5 days of extensive handling, on the 13th day, mice were placed into a completely new context (environment ”B”). Here, they displayed normal exploratory behavior without freezing, indicating that their previously established fear memories were specific for environment ”A”. In environment ”B” they received 4 foot-shocks (2 mA, 2 s) with a 30 second inter-shock interval without laser stimulation. On day 14, mice were placed back to environment ”B” to analyze their freezing behavior.
B: ChR2 mice spent significantly more time freezing in environment ”B” than in environment ”A”, indicating that NI successfully inhibited contextual fear memory formation in environment ”A”. Population data for freezing (in % of total time) are as follows (median [25%-75% quartiles]): ChR2 in environment ”A”: 1.22 [0.00-2.45], ChR2 in environment ”B”: 6.34 [2.22-12.85] (*: p=0.018, Wilcoxon signed-rank test). Freezing levels of ChR2 and CTRL mice were not different in environment ”B”, indicating that both groups of mice were capable of forming contextual fear memories. Population data for freezing (in % of total time) are as follows (median [25%-75% quartiles]): ChR2 in environment ”B”: 6.34 [2.22-12.85], CTRL in environment ”B”: 12.12 [5.78-16.80] (n.s: non-significant, p=0.417, Mann-Whitney U-test). Graph shows individual data (dots) and medians (lines).

Table S1. Primary antibodies and retrograde tracers

Antigen	Host	Dilution	Source	Catalog number
Calbindin	Rabbit	1:2000	Kind gift from K. Baimbridge	-
choline acetyltransferase (ChAT)	Mouse	1:1000	Kind gift from C. Cozzari	-
Choleratoxin B subunit	Goat	1:20000	List Biologicals	#703
Choleratoxin B subunit	Mouse	1:2000	Abcam	ab1003
eGFP	Chicken	1:1000	Abcam	ab13970
eGFP	Chicken	1:2000	ThermoFisher Scientific	A10262
eGFP	Rabbit	1:1000	ThermoFisher Scientific	A11122
FluoroGold	Rabbit	1:500	Chemicon	AB153-i
GABA-A-g2	Rabbit	1:1000	Synaptic Systems	224 003
Gephyrin	Mouse	1:100	Synaptic Systems	147 021
Gephyrin	Rabbit	1:300-1:2000	Synaptic Systems	147 008
M2	Rat	1:500	Chemicon	MAB367
mCherry	Rabbit	1:5000	BioVision	5993-100
mGluR1a	Rabbit	1:2000	ImmunoStar	24426
Parvalbumin	Guinea pig	1:10000	Synaptic Systems	195 004
Parvalbumin	Rabbit	1:2000	Kind gift from K. Baimbridge	-
Relaxin-3	Mouse	1:20-1:1000	Provided by A.L. Gundlach	-
RFP	Rat	1:2000-1:5000	Chromotek	5F8
Serotonin	Rabbit	1:10000	ImmunoStar	20080
Somatostatin	Rabbit	1:1000	Acris/OriGene	AP33464SU-N
Somatostatin	Rat	1:300-1:1000	Chemicon	MAB354
tyrosine hydroxylase (TH)	Mouse	1:2000	ImmunoStar	22941
vesic. acetylcholine transporter (vAchT)	Goat	1:10000	ImmunoStar	24286
vesicular GABA transporter (vGAT)	Guinea pig	1:2000	Synaptic Systems	131 004
vesicular glutamate transporter type 2 (vGluT2)	Guinea pig	1:2000	Synaptic Systems	135 404
(vGluT3)	Rabbit	1:500	Synaptic Systems	135 203
Choleratoxin B subunit		0,5%	List Biologicals	#104
FluoroGold		2%	FluoroChrome Inc.	-

Table S2. Characterization of the primary antibodies and retrograde tracers used.

Antigen	Host	Specificity	Characterized in
Calbindin	Rabbit	The antibody recognizes one major broad band of the expected molecular weight (28 kDa) on western blots from rat cerebellum samples and immunostaining was abolished by preadsorption with the immunogen.	[1]
choline acetyltransferase (ChAT)	Mouse	Staining is typical for cholinergic cells; complete overlap of staining with eYFP-positive cells in ChAT-iRES-Cre mice injected with AAV-EF1a-DIO-eYFP.	[2,3]
Choleratoxin B subunit	Goat	No staining in non-injected mice.	[4]
Choleratoxin B subunit	Mouse	No staining in non-injected mice.	[5]
eGFP (Abcam)	Chicken	No staining in mice not injected with eGFP-expressing virus.	Information of the distributor
eGFP (Thermo Fisher Sci.)	Chicken	No staining in mice not injected with eGFP-expressing virus.	Information of the distributor
eGFP	Rabbit	No staining in mice not injected with eGFP-expressing virus.	Information of the distributor
FluoroGold	Rabbit	No staining in non-injected mice.	[6]
GABA-A-γ2	Rabbit	No staining in GABA-A-γ2 floxed mice in areas injected with AAV-Cre (conditional knockout); extracellular epitope.	[7]
Gephyrin	Mouse	KO verified.	Information of the distributor
Gephyrin	Rabbit	KO verified.	Information of the distributor
M2	Rat	KO verified.	[8]
mCherry	Rabbit	No staining in mice not injected with mCherry-expressing virus.	Information of the distributor
mGluR1a	Rabbit	Several antibodies for different epitopes gave the same labeling pattern.	[9]
Parvalbumin	Guinea pig	Labels the same cell populations in the brain as other antibodies to parvalbumin.	Information of the distributor, [10]
Parvalbumin	Rabbit	Labels the same cell populations in the brain as other antibodies to parvalbumin.	[11,12]
Relaxin-3	Mouse	KO verified.	[13]
RFP	Rat	No staining in mice not injected with mCherry-expressing virus.	Information of the distributor
Serotonin	Rabbit	Staining is typical for serotonergic neurons, complete overlap with TpH-staining.	[14,15]

Somatostatin	Rabbit	Labels the same neuron populations in the brain as other antibodies to somatostatin.	[16]
Somatostatin	Rat	Labels the same neuron populations in the brain as other antibodies to somatostatin.	[17]
TH	Mouse	Staining is typical for TH-positive neurons.	[18]
vesicular acetylcholine transporter (vAchT)	Goat	Complete overlap with ChAT staining.	[3]
vesicular GABA transporter (vGAT)	Guinea pig	KO verified.	Information of the distributor
vesicular glutamate transporter type 2 (vGluT2)	Guinea pig	The antibody recognizes one major broad band of the expected molecular weight (65 kDa) on western blots of a synaptic vesicle fraction of rat brain and immunostaining was abolished by preadsorption with the immunogen.	Information of the distributor, [19]
vesicular glutamate transporter type 3 (vGluT3)	Rabbit	KO verified.	Information of the distributor
Choleratoxin B subunit		Retrograde tracer.	[20]
FluoroGold		Retrograde tracer.	[20]

Footnote: [1] A.M.J. Buchan, K.G. Baimbridge, Peptides 9 (1988) 333–338. [2] A. Chédotal et al. Brain Res. 646 (1994) 181–193. [3] V.T. Takács et al., Nat. Commun. 9 (2018). [4] P.J.W.C. Dederen et al., Histochem. J. 26 (1994) 856–862. [5] K.T. Hamorsky et al. PLoS Negl. Trop. Dis. 7 (2013). [6] C. Varga et al. J. Neurosci. 22 (2002) 6186–6194. [7] Z. Rovo et al. J. Neurosci. 34 (2014) 7137–7147. [8] K.A. Kohlmeier et al. J. Neurophysiol. 108 (2012) 2751–2766. [9] R.G.E. Notenboom et al., Brain 129 (2006) 96–107. [10] L. Massi et al., J. Neurosci. 32 (2012) 16496–16502. [11] F. Condé et al. J. Comp. Neurol. 341 (1994) 95–116. [12] F. Mascagni et al. Neuroscience 158 (2009) 1541–1550. [13] S. Ma et al. J. Physiol. 591 (2013) 3981–4001. [14] S.R. Fox, E.S. Deneris, J. Neurosci. 32 (2012) 7832–42. [15] S. KE et al., Brain Struct. Funct. 222 (2016) 287–299. [16] F. Antonucci et al. J. Neurosci. 32 (2012) 1989–2001. [17] Y. Kubota et al. Cereb. Cortex 21 (2011) 1803–1817. [18] M. Chermenina et al. Parkinsons. Dis. 1 (2015). [19] J. Broms et al. J Comp Neurol 523 (2016) 359–380. [20] J.L. Lanciego et al. J. Chem. Neuroanat. 42 (2011) 157–183.

Table S3. Secondary antibodies.

Raised in (species)	Raised against (species)	Conjugated with	Dilution	Source	Catalog number
Chicken	Rat	Alexa 647	1:500	ThermoFisher Scientific	A21472
Donkey	Rabbit	Alexa 647	1:500	Jackson Immunoresearch	711-605-152
Donkey	Mouse	Alexa 647	1:500	Jackson Immunoresearch	715-605-151
Donkey	Guinea pig	Alexa 647	1:500	Jackson Immunoresearch	706-605-148
Goat	Chicken	Alexa 488	1:1000	ThermoFisher Scientific	A11039
Donkey	Chicken	Alexa 488	1:300	Jackson Immunoresearch	703-545-155
Donkey	Goat	Alexa 488	1:500	ThermoFisher Scientific	A11055
Donkey	Rabbit	Alexa 488	1:1000	ThermoFisher Scientific	A21206
Donkey	Mouse	Alexa 488	1:500	ThermoFisher Scientific	A21202
Goat	Guinea pig	Alexa 488	1:500	ThermoFisher Scientific	A11073
Donkey	Goat	Alexa 594	1:500	ThermoFisher Scientific	A11058
Donkey	Guinea pig	Cy3	1:500	Jackson Immunoresearch	706-166-148
Donkey	Rabbit	Alexa 594	1:500	ThermoFisher Scientific	A21207
Donkey	Rat	Alexa 594	1:500	ThermoFisher Scientific	A21209
Donkey	Guinea pig	Alexa 594	1:500	Jackson Immunoresearch	706-585-148
Donkey	Mouse	Alexa 594	1:500	ThermoFisher Scientific	A21203
Goat	Chicken	biotinylated	1:200	Vector Laboratories	BA-9010
Goat	Rat	biotinylated	1:1000	Jackson Immunoresearch	112-066-062
Donkey	Mouse	biotinylated	1:1000	Jackson Immunoresearch	715-066-151
Donkey	Rabbit	biotinylated	1:1000	Jackson Immunoresearch	711-065-152
Goat	Rat	Horseradish peroxidase (ImmPress)	1:3	Vector Laboratories	MP-7444
Horse	Mouse	Horseradish peroxidase (ImmPress)	1:3	Vector Laboratories	MP-7402
Goat	Mouse	0.8 nm gold	1:50	Aurion	800 022
Goat	Rabbit	1.4 nm gold	1:100	Nanoprobes	#2004
	streptavidin	Alexa 594	1:500	ThermoFisher Scientific	S11227

Table S4. Primary and secondary antibody combinations used in immunofluorescence experiments.

Mouse strain	Primary antibodies used	Secondary antibodies used
C57Bl/6 WT	rabbit-anti-FluoroGold goat-anti-Choleratoxin B	Alexa 488-conjugated donkey-anti-rabbit Alexa 594-conjugated donkey-anti-goat
C57Bl/6 WT	rabbit-anti-FluoroGold goat-anti-Choleratoxin B mouse-anti-Relaxin-3	Alexa 488-conjugated donkey-anti-rabbit Alexa 594-conjugated donkey-anti-goat Alexa 647-conjugated donkey-anti-mouse
C57Bl/6 WT	guinea pig-anti-Parvalbumin mouse-anti-Relaxin-3 rabbit-anti-Gephyrin	Alexa 488-conjugated goat-anti-guinea pig Alexa 594-conjugated donkey-anti-mouse Alexa 647-conjugated donkey-anti-rabbit
ChAT-iRES-Cre; vGluT2-iRES-Cre	chicken-anti-eGFP (ThermoFisher) mouse-anti-Relaxin-3 rabbit-anti-Gephyrin	Alexa 488-conjugated goat-anti-chicken Alexa 594-conjugated donkey-anti-mouse Alexa 647-conjugated donkey-anti-rabbit
SOM-iRES-Cre	chicken-anti-eGFP (ThermoFisher) mouse-anti-Relaxin-3 rabbit-anti-Gephyrin	Alexa 488-conjugated goat-anti-chicken Alexa 594-conjugated donkey-anti-mouse Alexa 647-conjugated donkey-anti-rabbit
vGAT-Cre	chicken-anti-eGFP (ThermoFisher) rat-anti-somatostatin rabbit-anti-mGluR1alpha	Alexa 488-conjugated goat-anti-chicken Alexa 594-conjugated donkey-anti-rat Alexa 647-conjugated donkey-anti-rabbit
vGAT-Cre	chicken-anti-eGFP (ThermoFisher) mouse-anti-Relaxin-3 rabbit-anti-parvalbumin	Alexa 488-conjugated goat-anti-chicken Alexa 594-conjugated donkey-anti-mouse Alexa 647-conjugated donkey-anti-rabbit
vGAT-iRES-Cre, GlyT2-iRES-Cre, vGluT2-iRES-Cre	chicken-anti-eGFP (ThermoFisher)	Alexa 488-conjugated goat-anti-chicken
vGAT-tdTomato	mouse-anti-tyrosine hydroxylase rabbit-anti-serotonin	Alexa 488-conjugated donkey-anti-mouse Alexa 647-conjugated donkey-anti-rabbit
vGAT-Cre	rabbit-anti-eGFP	Alexa 488-conjugated donkey-anti-rabbit
vGAT-Cre	chicken-anti-eGFP (Abcam)	Alexa 488-conjugated donkey-anti-chicken
vGAT-Cre	rat-anti-RFP	Alexa 594-conjugated donkey-anti-rat
vGAT-Cre	chicken-anti-eGFP (ThermoFisher) rat-anti-RFP	Alexa 488-conjugated goat-anti-chicken Alexa 594-conjugated donkey-anti-rat
vGAT-Cre	mouse-anti-ChAT rabbit-anti-mCherry	Alexa 488-conjugated donkey-anti-mouse Alexa 594-conjugated donkey-anti-rabbit
vGAT-Cre	guinea pig-anti-Parvalbumin rat-anti-RFP rabbit-anti-Calbindin	Alexa 488-conjugated goat-anti-guinea pig Alexa 594-conjugated donkey-anti-rat Alexa 647-conjugated donkey-anti-rabbit

vGAT-Cre	rat-anti-RFP guinea pig-anti-vGluT2	Alexa 594-conjugated donkey-anti-rat Alexa 647-conjugated donkey-anti-guinea pig
vGAT-Cre	goat-anti-vAchT rat-anti-RFP	Alexa 488-conjugated donkey-anti-goat Alexa 594-conjugated donkey-anti-rat
vGAT-Cre	rat-anti-RFP rabbit-anti-vGluT3	Alexa 594-conjugated donkey-anti-rat Alexa 647-conjugated donkey-anti-rabbit
vGAT-Cre	chicken-anti-eGFP (ThermoFisher) mouse-anti-Relaxin-3 guinea pig-anti-vGAT	Alexa 488-conjugated goat-anti-chicken Alexa 594-conjugated donkey-anti-mouse Alexa 647-conjugated donkey-anti-guinea pig
vGAT-Cre	chicken-anti-eGFP (ThermoFisher) guinea pig-anti-vGAT mouse-anti-Relaxin-3	Alexa 488-conjugated goat-anti-chicken Cy3-conjugated donkey-anti-guinea pig Alexa 647-conjugated donkey-anti-mouse
vGAT-Cre	rabbit-anti-eGFP goat-anti-Choleratoxin B	Alexa 488-conjugated donkey-anti-rabbit Alexa 594-conjugated donkey-anti-goat
vGAT-Cre	rabbit-anti-eGFP goat-anti-Choleratoxin B rat-anti-M2 receptor	Alexa 488-conjugated donkey-anti-rabbit Alexa 594-conjugated donkey-anti-goat Alexa 647-conjugated chicken-anti-rat
vGAT-Cre	chicken-anti-eGFP (ThermoFisher) Alexa 594-conjugated Streptavidin rat-anti-somatostatin	Alexa 488-conjugated donkey-anti-rabbit Alexa 594-conjugated Streptavidin Alexa 647-conjugated donkey-anti-rat
vGAT-Cre	chicken-anti-eGFP (ThermoFisher) Alexa 594-conjugated Streptavidin rabbit-anti-somatostatin	Alexa 488-conjugated donkey-anti-rabbit Alexa 594-conjugated Streptavidin Alexa 647-conjugated donkey-anti-rabbit

Table S5. Primary and secondary antibody combinations used in the double immunogold-immunoperoxidase and in the double immunoperoxidase experiments.

C57Bl/6 WT	mouse-anti-Relaxin-3 rabbit-anti-Gephyrin	biotinylated donkey-anti-mouse 1.4 nm gold-conjugated goat-anti-rabbit
C57Bl/6 WT	mouse-anti-Relaxin-3 rabbit-anti-GABA-A-g2	biotinylated donkey-anti-mouse 1.4 nm gold-conjugated goat-anti-rabbit
vGAT-Cre	rabbit-anti-mCherry mouse-anti-Gephyrin	biotinylated donkey-anti-rabbit 0.8 nm gold-conjugated goat-anti-mouse
vGAT-Cre	rat-anti-RFP rabbit-anti-GABA-A-g2	biotinylated goat-anti-rat 1.4 nm gold-conjugated goat-anti-rabbit
vGAT-tdTomato	chicken-anti-eGFP (ThermoFisher) rat-anti-RFP	biotinylated goat-anti-chicken ImmPress goat-anti-rat
vGAT-Cre	chicken-anti-eGFP (ThermoFisher) rat-anti-somatostatin	biotinylated goat-anti-chicken ImmPress goat-anti-rat
vGAT-Cre	chicken-anti-eGFP (ThermoFisher) mouse-anti-Choleratoxin B	biotinylated goat-anti-chicken ImmPress horse-anti-mouse

Table S6. Quantification of monosynaptically-labeled neurons with rabies virus in the different brain areas projecting to GABAergic NI neurons.

Brain Area/Nucleus	Median %	Estimation of cell numbers per brain area			Behavioral relevance	References for behavioral relevance
		Mouse 1	Mouse 2	Mouse 3		
Prefrontal cortex	2,6%	174	654	138	fear behavior, reward, aversion	[1,2]
Cingulate cortex	1,4%	210	156	72	negative outcome of choice, aversion	[3]
Secondary motor cortex	1,3%	102	198	72	adaptive choice behavior, linking sensory cues to motor actions	[4]
Medial septum + Ventral limb of the diagonal band of Broca	1,3%	150	192	102	theta generation, episodic memory, sleep-wake cycles, motor control	[5–7]
Horizontal limb of the diagonal band of Broca + Substantia Innominata + nucleus basalis	1,3%	156	138	102	unexpected events with emotional valence	[8]
Lateral preoptic area	1,2%	54	186	162	aversion, reward system, CRH input into NI	[9]
Lateral habenula	4,1%	162	636	342	aversion, reward system	[9–11]
Zona incerta	2,3%	198	354	132	fear, freezing, attention, motor control	[12–14]
Lateral hypothalamus	4,3%	228	678	234	feeding-related reward behavior	[15–17]
Posterior hypothalamus	2,3%	276	276	138	theta rhythm, spatial memory	[18,19]
Mammillary body/ supramammillary	5,0%	600	960	60	motor control (head direction), memory formation, REM sleep	[19–22]
Periaqueductal grey	3,8%	696	390	198	freezing behavior	[23]
Ventral tegmental area	1,7%	204	66	96	reward processing, aversion	[2]
Mesencephalic reticular formation	1,5%	306	240	6	movement initiation	[24]
Dorsal raphe	3,8%	516	276	198	reward-related behavior, sleep-wake cycles	[25,26]
Median raphe	20,2%	2022	3156	1224	fear memory consolidation, anxiety and fear	[27,28]
Nucleus pontis oralis	6,3%	414	984	600	REM sleep, theta generation	[29,30]
Isthmic reticular formation	1,3%	42	210	108	movement initiation	[24]
Anterior/ventral tegmental nucleus (Gudden)	2,3%	300	102	120	REM sleep, theta generation, memory, motor control (head direction)	[31–34]
Laterodorsal tegmental nucleus	8,0%	954	N/A	N/A	reward processing (cocaine addiction)	[2,35]
Dorsomedial tegmental area	1,7%	444	258	78	REM sleep	[36]
Nucleus pontis caudalis	3,9%	462	636	114	motor control (movement initiation, acoustic startle, eye movement), REM sleep	[29,37,38]
Medial parabrachial nucleus	1,4%	168	42	84	taste perception (flavor avoidance), REM-NREM sleep-stage transitions	[39,40]
Nucleus prepositus	1,1%	312	168	12	motor control (head direction)	[41,42]
Gigantocellular nucleus	4,2%	504	678	102	sleep-wake cycles, motor control (REM atonia, emotional movement)	[40,43,44]
TOTAL	88,3%	11982	15630	5238		

Footnote: [1] R.R. Rozeske et al., Brain Behav. 14 (2015) 22–36. [2] S. Lammel et al., Nature 491 (2012) 212–217. [3] T. Kawai et al., Neuron 88 (2015) 792–804. [4] F. Barthas, A.C. Kwan, Trends Neurosci. 40 (2017) 181–193. [5] M. Vandecasteele et al., Proc. Natl. Acad. Sci. 111 (2014) 13535–13540. [6] R. Boyce et al., Science (80-.). 352 (2016) 812. [7] F. Fuhrmann et al., Neuron 86 (2015) 1253–1264. [8] B. Hangya et al., Cell 162 (2015) 1155–1168. [9] D.J. Barker et al., Cell Rep. 21 (2017) 1757–1769. [10] A.M. Stamatakis, G.D. Stuber, Nat. Neurosci. 15 (2012) 1105–1107. [11] T.C. Jhou et al., Neuron 61 (2009) 786–800. [12] X.L. Chou et al., Nat. Commun. 9 (2018) 1–12. [13] S. Chometton et al., Brain Struct. Funct. 222 (2017) 2507–2525. [14] G.D.R. Watson et al., J. Neurosci. 35 (2015) 9463–9476. [15] J.-J. Liu et al., J. Neurosci. 37 (2017) 11854–11866. [16] M. Fattahi et al., Addict. Biol. (2018). [17] A.G. Choudhary et al., Brain Struct. Funct. 223 (2018) 1313–1328. [18] R. Bocian et al., Hippocampus 26 (2016) 1354–1369. [19] B.E. Gutiérrez-Guzmán et al., Eur. J. Pharmacol. 682 (2012) 99–109. [20] C.M. Dillingham et al., Neurosci. Biobehav. Rev. 54

(2015) 108–119. [21] S.D. Vann, J.P. Aggleton, Nat. Rev. Neurosci. 5 (2004) 35–44. [22] P.H. Luppi et al., Curr. Opin. Neurobiol. 44 (2017) 59–64. [23] P. Tovote et al., Nature, Press 534 (2016) 206–212. [24] T.K. Roseberry et al., Cell 164 (2016) 526–537. [25] M. Luo et al., Learn Mem 22 (2015) 452–460. [26] J.M. Monti, Sleep Med. Rev. 15 (2011) 269–281. [27] D. V Wang et al., Nat. Neurosci. 18 (2015) 728–35. [28] T.G. Andrade et al., J. Psychopharmacol. 27 (2013) 1107–15. [29] L.D. Sanford et al., J. Neurophysiol. 90 (2003) 938–945. [30] R.P. Vertes, B. Kocsis, Neuroscience 81 (1997) 893–926. [31] P. Torterolo et al., Brain Res. 944 (2002) 184–189. [32] M.H. Bassant et al., Hippocampus 11 (2001) 809–813. [33] P.E. Sharp et al., Behav. Neurosci. 115 (2001) 571–588. [34] S.D. Vann, Brain 132 (2009) 2372–2384. [35] K. Kaneda, Eur. J. Neurosci. (2018) 0–1. [36] S. Valencia Garcia et al., Brain Struct. Funct. 223 (2018) 2733–2751. [38] J. Márquez-Ruiz, M. Escudero, Sleep 33 (2010) 1517–1527. [39] M.L. De La Torre, Á. Agüero, Exp. Brain Res. 194 (2009) 207–218. [40] Y. Hayashi et al., Science (80). 350 (2015) 957–962. [41] W.N. Butler et al., Curr. Biol. 27 (2017) 1259–1267. [42] W.N. Butler, J.S. Taube, J. Neurosci. 35 (2015) 2547–2558. [43] E.M. Martin et al., J. Comp. Neurol. 519 (2011) 2574–2593. [44] Y.-Y. Lai et al., J. Neurophysiol. 104 (2010) 2024–2033.

Table S7. Immunochemical characterization of basal forebrain neurons (medial septum, vertical and horizontal limbs of the diagonal bands of Broca and substantia innominata pooled) monosynaptically projecting onto GABAergic NI neurons.

	Number	Percentage to total number of cells labeled
Total counted basal forebrain neurons for analyzing ChAT-positivity	35	2,86%
ChAT-positive neurons (n=1 mouse)	1	
Total counted basal forebrain neurons for analyzing PV-positivity	97	18,56%
PV-positive neurons (n=3 mice)	18	
Total counted basal forebrain neurons for analyzing CB-positivity	97	5,15%
CB-positive neurons (n=3 mice)	5	